Characteristics of Vertical Air Motion in Isolated Convective Clouds

Jing Yang[1], Zhien Wang[1], Andrew J. Heymsfield[2] and Jeffrey R. French[1]

[1] {Department of Atmospheric Science, University of Wyoming, Laramie, WY}

[2] {National Center for Atmospheric Research, Boulder, CO}

Correspondence to: Zhien Wang (zwang@uwyo.edu)

Abstract

The vertical velocity and air mass flux in isolated convective clouds are statistically analyzed using aircraft in-situ data collected from three field campaigns: High-Plains Cumulus (HiCu) conducted over the mid-latitude High Plains, COnvective Precipitation Experiment (COPE) conducted in a mid-latitude coastal area, and Ice in Clouds Experiment-Tropical (ICE-T), conducted over a tropical ocean. This study yields the following results. (1) Small-scale updrafts and downdrafts (< 500 m in diameter) are frequently observed in the three field campaigns, and they make important contributions to the total air mass flux. (2) The probability density functions (PDFs) and profiles of the vertical velocity are provided. The PDFs are exponentially distributed. The updrafts generally strengthen with height. Relatively strong updrafts (> 20 m s^{-1}) were sampled in COPE and ICE-T. The downdrafts are stronger in HiCu and COPE than in ICE-T. (4)

The PDFs of the air mass flux are exponentially distributed as well. The maximum air mass flux in updrafts is of the order 10^4 kg m^{-1} s^{-1}. The air mass flux in the downdrafts is typically a few times smaller in magnitude than that in the updrafts. Since this study only deals with isolated convective clouds, and there are many limitations and sampling issues in aircraft in-situ measurements, more observations and simulations are needed to better explore the vertical air motion in convective clouds.

1. Introduction

Convective clouds are an important component of the global energy balance and water cycle because they dynamically couple the planetary boundary layer to the free troposphere through vertical heat, moisture and mass transport (Arakawa, 2004; Heymsfield et al., 2010; Wang and Geerts, 2013). The vertical velocity determines the vertical transport of cloud condensate, the cloud top height and the detrainment into anvils, which further impact the radiative balance (Del Genio et al., 2005). Vertical velocity also has significant impact on the aerosol activation, droplet condensation and ice nucleation in convective clouds, which control the cloud life cycle and precipitation efficiency.

In order to reasonably simulate convective clouds, the vertical air velocity must be parameterized reliably in numerical weather prediction models (NWPMs) and global circulation models (GCMs) (Donner et al., 2001; Tonttila et al., 2011; Wang and Zhang, 2014). However, the complexity of the vertical velocity structure in convective clouds makes the parameterization non-straightforward (Wang and Zhang, 2014). Observations show that in most of the convective clouds the vertical velocity is highly variable, and consequently the detailed structure of

convection cannot be resolved in many models (Kollias et al., 2001; Tonttila et al., 2011). Additionally, using the same parameterization of vertical velocity for different grid resolutions may result in different cloud and precipitation properties (Khairoutdinov et al., 2009). Furthermore, poorly parameterized vertical velocity may result in large uncertainties in the microphysics; for instance, the cloud droplet concentration may be underestimated due to unresolved vertical velocity (Ivanova and Leighton, 2008). Vertical velocity simulated by models with horizontal resolutions down to a few hundred meters may be more realistic (e.g. Wu et al., 2009), but more observations are needed to evaluate this suggestion.

Aircraft in-situ measurement has been the most reliable tool enabling us to understand the vertical velocity in convective clouds and to develop the parameterizations for models. Early studies (e.g. Byers and Braham, 1949; Schmeter, 1969) observed strong updrafts and downdrafts in convective clouds; however, their results have a large uncertainty, because the aircrafts were not equipped with inertial navigation systems (LeMone and Zipser, 1980). In 1974, the Global Atmospheric Research Program (GARP) Atlantic Tropical Experiment (GATE) was conducted off the west coast of Africa, focusing on tropical maritime convections (Houze, 1981). A series of findings based on the aircraft data collected from the project was reported. For example, the accumulated probability density functions (PDFs) of vertical velocity and diameter of the convective cores are lognormal distributed. The updrafts and downdrafts in GATE (tropical maritime clouds) were only one half to one third as strong as those observed in the Thunderstorm Project (continental clouds) (LeMone and Zipser, 1980; Houze, 1981). These findings stimulated later statistical studies of the vertical velocity in convective clouds. Jorgensen et al. (1985) found that the accumulated PDFs of vertical velocity in intense hurricanes were also lognormal distributed and the strength was similar to that in GATE, but the diameter of the convective

region was larger. Studies of the convective clouds over Taiwan (Jorgensen and LeMone, 1989) and Australia (Lucas et al., 1994) showed a magnitude of vertical velocity similar to that in GATE. Although the results from the Thunderstorm Project are suspect, the significantly stronger drafts reveal the possible difference between continental and tropical maritime convective clouds. Lucas et al. (1994) suggested that the water loading and entrainment strongly reduce the strength of updrafts in maritime convections. However, this underestimation of the updraft intensity may be also due to the sampling issues, e.g. penetrations were made outside the strongest cores (Heymsfield et al., 2010).

There are a few more recent aircraft measurements (e.g. Igau et al, 1999; Anderson et al., 2005), but the data are still inadequate to fully characterize the vertical velocity in convective clouds. In most of these earlier papers, the defined draft or draft core required a diameter no smaller than 500 m; this threshold excluded many narrow drafts with strong vertical velocity and air mass flux. In addition, the earlier studies used 1-Hz resolution data, which can resolve only the vertical velocity structures larger than a few hundred meters, but the narrow drafts may be important to the total air mass flux exchange and cloud evolution. Furthermore, previous aircraft observations for continental convective clouds were based only on the Thunderstorm Project; thus, new data are needed to study the difference between continental and maritime convections.

Remote sensing by means of, for example, wind profilers and radars is another technique which has often been used in recent years for studying the vertical velocity in convective clouds (e.g. Kollias et al., 2001; Hogan et al., 2009; Giangrande et al., 2013; Schumacher et al., 2015). Using profiler data, May and Rajopadhyaya (1999) analyzed the vertical velocity in deep convections near Darwin, Australia. They observed that the updraft intensified with height and that the maximum vertical velocity was greater than 15 m s^{-1}. Heymsfield et al. (2010) studied the

vertical velocity in deep convections using an airborne nadir-viewing radar. Strong updrafts were observed over both continental and ocean areas, with the peak vertical velocity exceeding 15 m s^{-1} in most of the cases and exceeding 30 m s^{-1} in a few cases. Zipser et al. (2006) used satellite measurements to find the most intense thunderstorms around the world; they applied a threshold updraft velocity greater than 25 m s^{-1} to identify intense convection. Collis et al. (2013) provides statistics of updraft velocities for different convective cases near Darwin, Australia using retrievals from scanning Doppler radars and a multifrequency profiler. Airborne volumetric Doppler radars have also been used to study the dynamic structure of convective clouds (e.g. Jorgensen and Smull 1993; Hildebrand et al. 1996; Jorgensen et al. 2000). Remote sensing has the advantage of being able to measure the vertically velocity at different heights simultaneously (Tonttila et al., 2011), and some of the techniques can detect the strongest updraft core in convective clouds (Heymsfield et al. 2010; Collis et al. 2013). Volumetric radars can also provide three-dimensional structure of air motion in convective clouds (Collis et al. 2013; Nicol et al. 2015; Jorgensen et al. 2000). However, remote sensing measurements are not as accurate as aircraft measurements, because many assumptions are needed to account for the contribution of hydrometeor fall speed in the observed Doppler velocity in order to ultimately estimate air velocity. In addition, ground-based radars can rarely provide good measurements over oceans, and airborne cloud radars often suffer from the attenuation and non-Rayleigh scattering in convective clouds. Therefore, in-situ measurements are still necessary in order to characterize the dynamics in convective clouds and to develop parameterizations for models.

The present study provides aircraft data analysis of the updrafts and downdrafts in mid-latitude continental, mid-latitude coastal and tropical maritime convective clouds using the fast-response in-situ measurements collected from three field campaigns: the High-Plains Cumulus (HiCu), the

COnvective Precipitation Experiment (COPE) and the Ice in Clouds Experiment-Tropical (ICE-T). All the clouds formed in isolation, but some of them merged as they evolved. Statistics of the vertical velocity and air mass flux are provided. The Wyoming Cloud Radar (WCR), onboard the aircraft, is used to identify the cloud top height, and high frequency (25-Hz) in-situ measurements of vertical velocity are used to generate the statistics. The major limitations of aircraft in-situ measurements are the aircraft maybe not able to sample the strongest part of convections due to safety concern, and it only provides the information of vertical air motion at single levels. These weaknesses need to be kept in mind in the following analyses. Section 2 describes the datasets and wind measuring systems. Section 3 presents the analysis method. Section 4 shows the results. Section 5 discusses the possible factors those interact with vertical air motions, and conclusions are given in Section 6.

2. Dataset and instruments

2.1 Dataset

The data used in the present study were collected from three field campaigns: HiCu, COPE and ICE-T. Vigorous convective clouds were penetrated during the three field campaigns, including mid-latitude continental, mid-latitude coastal, and tropical maritime convective clouds. These penetrations provide good quality measurements for studying the microphysics and dynamics in the convective clouds, as well as the interactions between the clouds and the ambient air. The locations of the three field campaigns are shown in Fig. 1. Information regarding the penetrations used in this study is summarized in Table 1.

The HiCu project was conducted mainly in Arizona and Wyoming (Fig. 1) from the 18th of July to the 5th of August, 2002, and from the 7th of July to the 31st of August, 2003 to investigate the microphysics and dynamics in convective clouds over mid-latitude High Plains. The University of Wyoming King Air (UWKA) was operated as the platform. In 2002 and 2003, 10 and 30 research flights were made, respectively. In this study, the 2002 HiCu and 2003 HiCu are analyzed together because they were both conducted over the High Plains and the sample size of 2002 HiCu is relatively small. Fast-response in-situ instruments and the Wyoming Cloud Radar (WCR, Wang et al., 2012) were operated during the field campaign to measure the ambient environment, cloud dynamics and microphysics as well as two-dimensional (2D) cloud structure. As shown in Table 1, penetrations in HiCu were made between 2 km and 10 km MSL. The sample size is relatively good below 8 km and relatively small above 8 km. The aircraft flew about 2000 km in clouds. In-situ measurements and WCR worked well in these flights; however, the upward-pointing radar was operated in less than half of the research flights, and thus only a sub-set of the cloud tops can be estimated. Fig. 2a(1–3) shows an example of the clouds sampled in HiCu, including WCR reflectivity, Doppler velocity and 25-Hz in-situ measurement of the vertical velocity. In HiCu, both developing and mature convective clouds were penetrated; some penetrations were near cloud top, while most of them were more than 1 km below cloud top. The typical WCR reflectivity is 0-15 dBZ in the convective cores due to strong Mie scattering at the WCR wavelength. From the Doppler velocity and the in-situ vertical velocity, we can see that, in both the developing and mature cloud, relatively strong updrafts and downdrafts were observed, and multiple updrafts and downdrafts existed in the same cloud. These drafts maybe strong for isolated convections, but not necessary strong compared to the strongest updrafts in mesoscale connective systems (MCSs). No soundings are available to measure the ambient environment in

HiCu, so we have to use aircraft measurements to estimate the convective available potential energy (CAPE). In some cases, the full CAPE cannot be calculated since the aircraft only flew at low levels (< 10 km MSL). The aircraft measurements suggest the CAPE in HiCu ranges from less than 100 J kg^{-1} to more than 500 J kg^{-1}.

The COPE project was conducted from the 3rd of July to the 21st of August, 2013 in Southwest England (Fig. 1). The UWKA was used to study the microphysics and entrainment in mid-latitude coastal convective clouds (Leon et al., 2015). Seventeen research flights were conducted; penetrations focused on regions near cloud top, which is verified based on the radar reflectivity from the onboard WCR. Since COPE was conducted in a coastal area, the convection initiation mechanism is different from that over a purely continental or ocean area. In addition, although the ambient air mainly came from the ocean, continental aerosols might be brought into clouds, since many of the convective clouds formed within the boundary layer, which further affects the microphysics and dynamics in the clouds. The measurements made in COPE include temperature, vertical velocity, liquid water content, and particle concentration and size distributions. The WCR provided excellent measurements of reflectivity and Doppler velocity. The downward Wyoming Cloud Lidar (WCL) was operated to investigate the liquid (or ice) dominated clouds. The typical WCR reflectivity is 5-20 dBZ in the convective cores. Between 0 km and 6 km, about 800 penetrations were made. Flight distance in cloud totaled about 1000 km. The sample sizes are relatively good between 2 km and 6 km, but relatively small between 0 km and 2 km. Examples of the penetrations are given in Fig. 2b(1–3). COPE has fewer penetrations than HiCu, and most of the penetrations are near the cloud top. Fig. 2b(2) reveals relatively simple structures of the updrafts and downdrafts in COPE compared to HiCu, but as shown by the 25-Hz in-situ vertical velocity measurement in Fig. 2b(3), there are still many complicated fine structures in

178 the vertical velocity distribution. The typical CAPE estimated from soundings in COPE was a
179 few hundred J kg^{-1}.

180 The ICE-T project was conducted from the 1st of July to the 30th of July, 2011 near St. Croix,
181 U.S. Virgin Islands (Fig. 1), with state-of-the-art airborne in situ and remote sensing
182 instrumentations, with the aim of studying the role of ice generation in tropical maritime
183 convective clouds. The NSF/NCAR C-130 aircraft was used during ICE-T to penetrate
184 convective clouds over the Caribbean Sea. Thirteen C-130 research flights were conducted
185 during the field campaign, with vigorous convective clouds penetrated. In-situ measurements
186 from ICE-T include the liquid and total condensed water contents, temperatures, vertical
187 velocities, and cloud and precipitating particle concentrations and size distributions. The WCR
188 was operated on seven research flights to measure the 2D reflectivity and Doppler velocity fields.
189 The typical WCR reflectivity in the convective cores is 10-20 dBZ. The aircraft flew more than
190 1500 km in clouds, and more than 650 cloud penetrations were made between 0 km and 8 km.
191 The sample sizes are good except between 2 km and 4 km (Table 1). Examples of the
192 penetrations are shown in Fig. 2c(1–3). During ICE-T, clouds in different stages were penetrated,
193 including developing, mature and dissipating, some near cloud top and some considerably below
194 cloud top. Updrafts up to 25 m s^{-1} updrafts were observed, the downdrafts in ICE-T are typically
195 weaker than those in HiCu and COPE. The vertical velocity structures are complicated, as
196 confirmed by both the Doppler velocity and the 25-Hz in-situ measurement. Weak updrafts and
197 downdrafts were also observed in the dissipating clouds. The typical CAPE in ICE-T was greater
198 than 2000 J kg^{-1}, which is larger than that in HiCu and COPE.

199 During the sampling of isolated convective clouds in the three field campaigns, we typically
200 aligned the central part of cloud to penetrate at the flight height, but still, the aircrafts might not

penetrate through the strongest part of convective core due to safety concern. In addition, aircraft in-situ measurements only provide the information of vertical air motion at single levels. Moreover, the clouds sampled are isolated convective clouds, MCSs were not sampled.. These limitations need to be kept in mind in interpreting results from the following analysis.

2.2 Wind measuring system

On both C-130 and UWKA, A Radome Five-Hole Gust Probe is installed for three-dimensional (3D) wind measurement**.** A Radome Five-Hole Gust Probe is an aircraft radome probe with five pressure ports installed in a "cross" pattern. Relative wind components (e.g. true air speed and flow angles) are sensed by a combination of differential pressure sensors attached to the five holes (Wendisch and Brenguier, 2013). Detailed calculation of relative wind components is described in Kroonenberg et al. (2008) and Wendisch and Brenguier (2013). The time response and the accuracy of the pressure sensors is about 25 Hz and 0.1 mb. The 3D wind vectors can be derived by taking out the aircraft motions from the relative wind measurement. On both C-130 and UWKA, the aircraft motion is monitored by a Honeywell LASEREF SM Inertial Reference System (IRS), with an accuracy of 0.15 m s^{-1} for vertical motion. Global Positioning System (GPS) was applied to remove the drift errors in the IRS position in all the three field campaigns (Khelif et al., 1998). The final vertical wind velocity product has an accuracy of about ±0.2 m s^{-1}, and a time response of 25 Hz. This uncertainty (±0.2 m s^{-1}) is a mean bias. For each output, the uncertainty is related to the true air speed, aircraft pitch angle, roll angle and ambient conditions. Therefore, the random error varies and could be larger than the mean bias. More information about the wind measurement on C-130 and UWKA can be found on the C-130 Investigator

Handbook (available on https://www.eol.ucar.edu/content/c-130-investigator-handbook) and UWKA Investigator Handbook (available on http://www.atmos.uwyo.edu/uwka/users/KA_InstList.pdf)

3. Analysis method

3.1 Identifying cloud using in-situ measurements

The Particle Measuring Systems (PMS) Two-Dimensional Cloud (2D-C) Probe and the Forward Scattering Spectrometer Probe (FSSP) are often used to characterize cloud microphysics (e.g. Anderson et al., 2004), although different thresholds of 2D-C and FSSP concentrations are usually used to identify the edge of a cloud. In this paper, we also use FSSP and 2D-C probes to find the cloud edges. In order to find a reasonable threshold for identifying cloudy air, we first use the WCR reflectivity to identify the clouds and the cloud-free atmosphere; for those regions we then plot the particle concentrations measured by FSSP and 2D-C in order to determine the reasonable thresholds, and we apply the thresholds of particle concentrations to all the research flights without WCR.

To identify clouds using WCR, the six effective range gates nearest to the flight level (three above and three below) are chosen in each beam. Any beam in which the minimum reflectivity at the six gates exceeds -30 dBZ[1] is identified as in cloud.

[1] Based on the reflectivity measured in cloud-free air, the noise level of WCR reflectivity is -32 dBZ at a range of 500 m and -28 dBZ at a range of 1000 m. In this study, we choose -30 dBZ as the threshold to identify cloud. This threshold (-30 dBZ) is examined for all three field campaigns.

241 Fig. 3 shows the occurrence distribution as a function of the particle concentrations measured by
242 FSSP versus the concentrations of the particles ≥ 50 μm in diameter measured by 2D-C in the
243 clouds identified by WCR reflectivity. From the figure, we can see that the FSSP concentration
244 ranges from 0.01 cm^{-3} to 1000 cm^{-3}, and the 2D-C concentration ranges from 0.1 L^{-1} to 10000 L^{-1}.
245 Generally, shallow clouds have relatively higher concentrations of small particles and lower
246 concentration of particles larger than 50 μm. In deeper convective clouds, high concentrations
247 can be seen for both small and large particles. The FSSP concentrations in cloud-free air are
248 found to be 2 cm^{-3} at most, and the FSSP concentrations measured below the lifting condensation
249 level (LCL), where precipitating particles dominated, are lower than 2 cm^{-3}, as well. Therefore, 2
250 cm^{-3} is selected as the concentration threshold to identify clouds based on the FSSP
251 measurements, as shown by the dashed line in Fig. 3. However, in some clouds (e.g. pure ice
252 clouds), the FSSP concentration could be lower than 2 cm^{-3}, and 2D-C concentrations are needed
253 to identify these cold clouds. We chose a 1 L^{-1} 2D-C concentration for particles ≥ 50 μm as the
254 second threshold to identify cloud, as shown by the dotted line in Fig. 3. In order to avoid
255 precipitating regions (below the LCL calculated from soundings), the second threshold is only
256 applied to penetrations at temperatures colder than 0 ºC; thus the cloud is defined as FSSP
257 concentration ≥ 2 cm^{-3} or 2D-C concentration ≥ 1 L^{-1}. At temperatures warmer than 0 ºC, the
258 FSSP concentrations in most of the convective clouds are higher than 2 cm^{-3}, so only the first
259 threshold is used.

260 Once a cloud is identified, the penetration details can be calculated, including the flight length,
261 the flight height, the cloud top height if WCR is available, and the penetration diameter. The
262 penetration diameter is calculated as the distance between the entrance and exit of a penetration.
263 In order to reject whirling penetrations and penetrations with significant turns, we require that

the diameter of a penetration be at least 90% of the flight length, so the cloud scale will not be significantly overestimated., Since the aircraft might not penetrate exactly through the center of a cloud, the actual cloud diameter may be larger than the penetration diameter. Based on WCR reflectivity images, there are no isolated convective clouds sampled larger than 20 km in diameter. There are a few penetrations longer than 20 km, but these clouds are more like part of MCSs, and so they are excluded from this study.

3.2 Defining updraft and downdraft

In previous studies of the vertical velocity based on in-situ measurements, the updraft and downdraft are often defined as an ascending or subsiding air parcel with the vertical velocity continuously ≥ 0 m s^{-1} in magnitude and ≥ 500 m in diameter (e.g. LeMone and Zipser, 1980; Jorgensen and LeMone, 1989; Lucas et al., 1994; Igau et al., 1999). In this study, we use a vertical velocity threshold of 0.2 m s^{-1}, that is, the draft has a vertical velocity continuously ≥ 0.2 m s^{-1} in magnitude, because ± 0.2 m s^{-1} is the accuracy of the instrument. Any very narrow and weak portion (diameter < 10 m and maximum vertical velocity < 0.2 m s^{-1} in magnitude) between two relatively strong portions is ignored, and the two strong portions are considered as one draft.

The diameter threshold (500 m) is not used in this paper, because drafts narrower than 500 m frequently occur and they make important contributions to the total air mass flux in the atmosphere and therefore they are necessarily to be considered in model simulations. Fig. 4 shows the PDFs of the diameters of all the updrafts and downdrafts sampled in HiCu, COPE and ICE-T. In all the panels, the diameters are exponentially distributed, the PDFs can be fitted using

$$f = \alpha \cdot |x|^{\beta} \cdot \exp(\gamma|x|) \qquad (1)$$

where f is the frequency and x is the diameter. The coefficients α, β and γ for each PDF is shown in each panel. This function will also be used to fit the PDFs of vertical velocity and air mass flux in the following analyses. Generally, as seen in Fig 4, the PDFs broaden with height increases for the three field campaigns; this is consistent with previous findings (LeMone and Zipser, 1980). The diameters of the updrafts are smaller in COPE compared to those sampled in HiCu and ICE-T, possibly because most of the penetrations are near cloud top. As shown in Fig. 4, many narrow drafts are observed. More than 85%, 90% and 74% of the updrafts are narrower than 500 m (dotted lines) in HiCu, COPE and ICE-T, respectively, and more than 90% of the downdrafts in all three field campaigns are narrower than 500 m. A threshold of 500 m in diameter would exclude many small-scale drafts, therefore, in this study all the drafts broader than 50 m (dashed lines) are included. The drafts narrower than 50 m are excluded because most of them are turbulence.

Fig. 5a shows the occurrence distributions as a function of the mean vertical velocity versus the diameter of the drafts with the vertical velocity continuously ≥ 0.2 m s^{-1} in magnitude. From the figure, it is noted that many drafts narrower than 500 m have quite strong vertical velocities. The maximum mean vertical velocity of these narrow drafts can reach 8 m s^{-1}, and the minimum mean vertical velocity in the downdrafts is –6 m s^{-1}. With such strong mean vertical velocity, narrow drafts could contribute noticeably to the total air mass flux. Fig. 5b presents the occurrence distributions as a function of the air mass flux versus the diameter of the drafts. The air mass flux is calculated as $\bar{\rho}\overline{w}D$ (LeMone and Zipser, 1980), where $\bar{\rho}$ is the mean air density at the measurement temperature, $\overline{w}$ is the mean vertical velocity and D is the diameter of each draft. Due to the limitation of aircraft measurements, the air mass flux is calculated using the

data from single line penetrations. This may introduce additional uncertainties in air mass flux estimations for these clouds and is a weakness of this study using aircraft data. Fig. 5b shows that the air mass flux in many drafts narrower than 500 m is actually larger than that in some of the broader drafts. The maximum value for these narrow updrafts reaches 4000 kg m^{-1} s^{-1}, and the minimum value for the downdrafts reaches –3000 kg m^{-1} s^{-1}. The normalized accumulated flux (red curves) reveals that the drafts narrower than 500 m (dotted horizontal lines) make very significant contributions to the total air mass flux. Calculations indicate that the updrafts narrower than 500 m contribute 20%–35% of the total upward flux, and that the downdrafts narrower than 500 m contribute 50%–65% of the total downward air mass flux. Drafts narrower than 50 m (dashed horizontal lines), which are excluded in this paper, contributes less than 5% of the total air mass flux.

In this study, we delineate three different groups of updraft and downdraft using three thresholds of air mass flux: 10 kg m^{-1} s^{-1}, 100 kg m^{-1} s^{-1} and 500 kg m^{-1} s^{-1} in magnitude. The air mass flux is used here to delineate the draft intensity because (1) air mass flux contains the information of both vertical velocity and draft size; (2) air mass flux can reveal the vertical mass transport through convection; and (3) air mass flux is an important component in cumulus and convection parameterizations (e.g. Tiedtke, 1989; Bechtold et al., 2001). The first designated group, the "weak draft," with air mass flux 10–100 kg m^{-1} s^{-1} in magnitude, contributes 10% of the total upward air mass flux and 10% of the total downward air mass flux. The "moderate draft," with air mass flux 100–500 kg m^{-1} s^{-1} in magnitude, contributes 25% of the total upward air mass flux and 40% of the total downward air mass flux. The "strong draft," where the air mass flux $\geq$ 500 kg m^{-1} s^{-1} in magnitude contributes 60% of the total upward air mass flux and 20% of the total downward air mass flux. The definitions of "weak", "moderate" and "strong" only apply for the

isolated convective clouds analyzed in this study, and are not necessarily appropriate for other convections (e.g. MCS). Drafts weaker than 10 kg m^{-1} s^{-1} are not analyzed because they are too weak and most of them are very narrow (Fig. 5b). The numbers of weak, moderate and strong updrafts and downdrafts sampled at 0–2 km, 2–4 km, 4–6 km, 6–8 km and 8–10 km MSL are shown in Table 2. Generally, weak and moderate drafts are more often observed than strong drafts. At most of the height ranges, more updrafts are observed than downdrafts.

Some researchers have defined a "draft core" by selecting the strongest portion in a draft. For example, LeMone and Zipser (1980) define an updraft core as an ascending air motion with vertical velocity continuously ≥ 1 m s^{-1} and diameter ≥ 500 m. This definition of a "draft core" is followed in a few more recent studies (e.g. Jorgensen and LeMone, 1989; Lucas et al., 1994; Igau et al., 1999). We too analyzed the vertical air motion characteristics in the stronger portion of the drafts considered here. However, we found that in many updrafts the strong portion where the vertical velocity is continuously ≥ 1 m s^{-1} dominates and contributes 80% of the total air mass flux, so the statistics of the vertical air motion characteristics in the stronger portion are very similar to those in the draft as a whole. Therefore, the present study focuses on "drafts" in which both weak and strong portions are included.

4. Results

4.1 Significance of drafts in different strengths

From the analysis above, we note that relatively small and weak updrafts are frequently observed in convective clouds. In this section, we provide further evidence to show the importance of the relatively weak updrafts in terms of air mass flux.

Fig. 6a shows the average number of updrafts as a function air mass flux observed in the three field campaigns. The solid, dashed and dotted lines represent the penetrations with different diameters. As shown in Fig. 6a, weak and moderate updrafts are more often observed than strong updrafts, and the numbers of updrafts are higher in longer penetrations. Since this is an average result, the number of updrafts could be smaller than 1 (e.g. many narrow penetrations do not have strong updrafts). Fig. 6b is similar to Fig. 6a but shows the occurrence frequency of updrafts with different air mass fluxes (i.e. the vertical axis in Fig. 6a is normalized). For the penetrations < 1 km, many of the clouds only have weak or moderate updrafts, and relatively strong updrafts are rarely observed. For penetrations of 1–10 km, the frequency of strong updrafts increases and the frequency of weak and moderate updrafts decreases. For even longer penetrations (>10 km), however, the frequency of weak updrafts increases again, indicating the increasing importance of weak updrafts.

Fig. 7 shows the average percentile contributions to the total upward air mass flux by the three different groups of updrafts as a function of penetration diameter. In Fig. 7a, all the penetrations are included. Since many narrow clouds have no strong updrafts in terms of air mass flux, the total air mass flux in these narrow clouds is mostly contributed by weak (red bar) and moderate (green bar) drafts. These narrow clouds may have a high vertical velocity but small air mass flux. As the diameter increases to 4 km, the contributions to total air mass flux from relatively weak updrafts (red bar) decrease, while those from stronger updrafts (blue bar) increase. For a penetration of 4 km, 80%–90% of the total upward mass flux is contributed by the strong

updrafts with air mass flux ≥ 500 kg m^{-1} s^{-1}. However, for the penetrations with diameter larger than 4 km, the contribution from relatively weak updrafts increases, probably because more weak updrafts exist in wider clouds (Fig. 6). This is more obvious in Fig. 7b, in which only the penetrations with at least one strong updraft are included. As the diameter increases from 400 m to 20 km, the contribution from the weak and moderate updrafts (red bars and green bars) increases from 2% to 20%. This suggests that as the cloud evolves and becomes broader (e.g. mature or dissipating stage), the weak and moderate updrafts are also important and therefore necessary to be considered in model simulations.

4.2 PDFs of vertical velocity and air mass flux

Fig. 8 shows the PDFs of the vertical velocity in the drafts sampled at 0–2 km, 2–4 km, 4–6 km and higher than 6 km in the three field campaigns. Columns (a), (b) and (c) represent the drafts with air mass flux ≥ 10 kg m^{-1} s^{-1}, ≥ 100 kg m^{-1} s^{-1} and ≥ 500 kg m^{-1} s^{-1} in magnitude, respectively; in other words, column (a) includes all the weak, moderate and strong of drafts, column (b) includes moderate and strong updrafts, and column (c) includes strong updrafts only. For statistical analysis, it is better to analyze different drafts together rather than separately. Since the aircraft might under sampled the strongest updraft cores, the tails of PDFs could biased low, but these PDFs still provide valuable information. In all the panels, the vertical velocities are exponentially distributed for both updrafts and downdrafts; the PDFs can be fitted using Eq. (1). From Fig. 8 we can see that at 0–2 km, the PDFs for both COPE and ICE-T are narrow. At 2–4 km, stronger updrafts and broader PDFs are observed in both COPE and ICE-T compared to those at 0–2 km; the maximum vertical velocity is about 15 m s^{-1}. In COPE, the downdrafts are

stronger than those in ICE-T, with the minimum vertical velocity as low as –10 m s^{-1}. For HiCu, the PDFs of the vertical velocity at 2–4 km are narrow, because the HiCu was conducted in the High Plains and the cloud bases are relatively high. At 4–6 km, the updrafts become stronger and the PDFs become broader in all the three field campaigns compared to those at lower levels, especially for COPE and ICE-T. Above 6 km, the PDFs for the updraft become broader in HiCu while they slightly narrow in ICE-T compared to those at 4–6 km. For the downdrafts, the PDFs broaden with height for all the three field campaigns. Generally, the PDFs of the vertical velocity are similar for the three columns. The main difference is found in the first bins of the vertical velocity (0–2 m s^{-1} and – 2–0 m s^{-1}): highest for column (a), which includes all the drafts with air mass flux $\geq$ 10 kg m^{-1} s^{-1} in magnitude, lowest for column (c), which only includes the strong drafts with air mass flux $\geq$ 500 kg m^{-1} s^{-1} in magnitude.

In Fig. 8, the updrafts are relatively stronger in ICE-T or COPE (maritime or coastal convective clouds) than in HiCu (pure continental convective clouds). But notice the aircrafts might under sample the strongest part of the convective cores. In addition, the PDFs are plotted as a function of MSL height, the relatively narrow PDFs in HiCu compared to COPE and ICE-T at the same height are possibly because of the higher cloud base in HiCu. Other than the sample issues, the convention triggering mechanism is also important to the updraft strength. The clouds sampled in the three field campaigns are all isolated convective clouds, the CAPE in HiCu was smaller than in COPE and ICE-T. Compared to GATE project, in which the clouds were also sampled over tropical ocean, the PDFs of the vertical velocity in ICE-T has a similar vertical dependence, broadening with height. But the PDFs are broader in ICE-T than those in GATE, and the maximum vertical velocity (25 m s^{-1}) in ICE-T is greater than that observed in GATE (15 m s^{-1}).

Notice in GATE, the in-situ measurements also have sampling issues. More measurements are needed to further evaluate the difference between maritime and continental convective clouds.

Fig. 9 shows the PDFs of the air mass flux for all the drafts sampled at 0–2 km, 2–4 km, 4–6 km and higher than 6 km. The PDFs are exponentially distributed for the three field campaigns at different heights, which can be fitted using Eq. (1). The coefficients for the fitted function are shown in each panel. In the three field campaigns, the PDFs of air mass flux have no obvious trend with height, although the PDFs of diameter and vertical velocity are broadening with height. The differences among the three field campaigns are small for weak and moderate drafts, and become slightly larger for relatively strong updrafts, which could be resulted from the sampling issues.

4.3 Profiles of vertical velocity and air mass flux

Fig. 10 is a Whisker-Box plot showing the profiles of the vertical velocity (a-c) and air mass flux (d-f) in the drafts based on the three defined thresholds of air mass flux. The solid box includes all the three different groups of drafts, the dashed boxes excludes the weak drafts, and the dotted boxes includes strong drafts only. The minimum, 10%, 50%, 90% and the maximum values are shown in each box. In each panel, the absolute values of the vertical velocities and air mass flux (except the minimum and maximum ones) are relatively small for the solid boxes.

In Fig. 10a-c, the three definitions of drafts show different intensities in the vertical velocities. Typically, the 10%, 50% and 90% values in the dotted boxes are 1–2 times larger in magnitude than those in the solid boxes. However, the profiles of the three definitions of drafts vary

similarly with height for each field campaign. In the updrafts sampled during HiCu (Fig. 10a), the maximum vertical velocity increases with height up to 8 km, then decreases with height; the 90% vertical velocity in the solid boxes increases from 4 m s^{-1} to 8 m s^{-1} between 0–10 km. The 10% and 50% vertical velocities in the solid boxes remain similar between 2–8 km then slightly increase at 8–10 km. In the downdrafts, the minimum vertical velocity decreases from –7 m s^{-1} to –12 m s^{-1} up to 8 km and increases to –9 m s^{-1} at 8–10 km. The 10%, 50 % and 90% values all slightly decrease with height. In the updrafts sampled during COPE (Fig. 10b), the maximum 10%, 50% and 90% vertical velocities increase with height, the maximum value is 23 m s^{-1}. The minimum vertical velocity in the downdrafts intensifies from –5 to –10 m s^{-1} with height up to 4 km, then remains similar at 4–6 km. In the updrafts sampled during ICE-T (Fig. 10c), the maximum vertical velocities increase with height from 5.5 m s^{-1} to 25 m s^{-1} up to 6 km, then slightly decreases at 6–8 km. The 90% value increases from 2 to 6 m s^{-1} between 0–4 km, then remains similar at higher levels. The 10% and 50% values do not show an obvious trend with height. In the downdrafts the minimum vertical velocity remains similar below 4 km, and decreases to –18 m s^{-1} between 4 km and 8 km. The 10%, 50% and 90% values tend to decrease or remain similar at first and then increase with height. The peak (~25 m s^{-1}) and the minimum (~-18 m s^{-1}) vertical velocities are observed at 4–6 km and 6–8 km, respectively.

To summarize, vertical velocity in the drafts varies differently with height in the three field campaigns. Stronger downdrafts are often observed in HiCu and COPE compared to those in ICE-T. The weak, moderate and strong drafts have similar variations with height, but the magnitudes are the smallest when including all the drafts and become larger if the weak drafts are excluded. The 10%, 50% and 90% vertical velocities in updrafts and downdrafts over tropical ocean (ICE-T) observed in this study generally have similar magnitudes to those shown in

previous studies (e.g. LeMone and Zipser, 1980; Lucus and Zipser, 1994). But strong updrafts (downdrafts) in excess of 20 m s^{-1} (–10 m s^{-1}) are also observed in this study, which are rarely reported in previous aircraft observations. This finding is consistent with recent remote sensing observations (e.g. Heymsfield et al., 2009). The updrafts and downdrafts in convective clouds over land shown in this study (HiCu) are weaker than those shown by Byers and Braham (1949) and Heymsfield et al. (2009), possibly because the clouds sampled in HiCu were isolated convective clouds over high plains, which could be different than deeper convective clouds from low elevations.

Fig. 10d-f shows the profiles the air mass flux statistics for the drafts sampled during the three field campaigns. As expected, the absolute values of the air mass flux are relatively small if all the drafts are included (dotted boxes), and become larger if the drafts with small air mass flux are excluded. However, the variations of the air mass flux with height are similar for the three different definitions in each panel. As determined by the three thresholds, the minimum absolute values in the solid boxes are about 10 times smaller than those in the dashed boxes and about 50 times smaller than those in the dotted boxed; for the 10%, 50%, 90% and the maximum absolute values, the differences among the three type of boxes become smaller. The air mass flux varies with height differently for the three field campaigns and do not have obvious trend with height. For updraft, the maximum air mass flux is of the order of 10^4 kg m^{-1} s^{-1}, and the median values for the three different types of boxes are typically ~100 kg m^{-1} s^{-1}, ~200 kg m^{-1} s^{-1} and ~1000 kg m^{-1} s^{-1}, respectively. The air mass flux in the downdrafts is a few times smaller in magnitude than those in the updrafts, but extreme strong downdraft on the order of 10^4 kg m^{-1} s^{-1} could be observed in some specific cases. Compared to previous studies, the air mass flux in this study shows similar magnitudes, but the vertical dependences are different. Lucas and Zipser (1994)

485 show that the convection off tropical Australia intensifies with height from 0 to 3 km, then
486 weakens with height in terms of air mass flux. Anderson et al. (2005) shows that updrafts and
487 downdrafts over the tropical Pacific Ocean intensify with height up to 4 km, then weaken at
488 higher levels. In contrast, this study shows the strongest updrafts and downdrafts in terms of air
489 mass flux were observed at higher levels.

490

491 **4.4 Composite structure of vertical velocity**

492 Fig. 11 shows the composite structure for the updrafts and downdrafts with air mass flux ≥ 10 kg
493 m^{-1} s^{-1} as a function of normalized scale. The 0 and 1 coordinates on the x-axis indicate the
494 upwind and downwind sides of the draft. Since we do not have continuous penetrations in a
495 single cloud, we have to statistically analyze the evolution of the draft structure. In Fig. 11, we
496 can see the normalized shape do not have significant change with height, the peak vertical
497 velocity is strengthening with height for all the three field campaigns. If the magnitude of the
498 vertical velocity is normalized, the structures of the updraft and downdraft at different heights
499 will be very similar. Connecting this figure to the PDFs of diameter (Fig. 4) and air mass flux
500 (Fig. 9), the results show statistically that the drafts were expanding (Fig. 4) and the vertical
501 velocity was strengthening (Fig. 11), but the air mass flux was not increasing with height (Fig. 9).
502 This reveals the complexity of the evolution of the drafts. Based on our datasets, there could be
503 different possibilities of the updraft evolution: 1) an updraft expands and the vertical velocity
504 weakens with height, 2) an updraft expands and the vertical velocity strengthens with height, 3)
505 an updraft splits to multiple updrafts and downdrafts, 4) two updrafts merged and become one

updrafts. In addition, entrainment/detrainment and water loading also have important impacts on the evolution of drafts in convective clouds.

In this composite analysis based on in-situ measurements, the penetration direction has no obvious impact on the vertical velocity structure, whether the aircraft penetrates along or across the horizontal wind (not shown). For convective cloud, wind shear has a large impact on the cloud evolution (Weisman and Klemp 1982); however, aircraft data are insufficient to reveal the wind shear impact, because each penetration is made at a single level and the aircraft does not always penetrate through the center of the draft. Remote sensing data can be helpful to study the two-dimensional or three-dimensional structures of the vertical velocity in convective clouds. For example, airborne radar with slant and zenith/nadir viewing beams can provide two-dimensional wind structure in convective clouds (e.g. Wang and Geerts, 2013). Volumetric radar (e.g. Collis et al. 2013, Jorgensen et al. 2000) can provide three-dimensional structure of air (or hydrometeor) motion. Thus, in-situ measurements as well as remote sensing measurements are needed to further analyze the wind shear impact.

4.5 Vertical air motion characteristics as clouds evolve

Fig. 12 shows the profiles of the vertical velocity (a-c) and the air mass flux (d-f) for the updraft and downdraft in the convective clouds with different cloud top heights (CTH). Here, all weak, moderate and strong updrafts are included. Different colors represent the clouds with different CTHs. These profiles can generally reveal the change of vertical velocity and air mass flux as the clouds evolve. The key point presented in Fig. 12a-c is that the peak vertical velocity is observed at higher levels as the clouds evolve. For clouds with CTHs lower than 4 km (red boxes), the

maximum vertical velocity is observed at 2–4 km. When the cloud become deeper, the vertical velocity and air mass flux are stronger at higher levels. This is to be expected, because all the data analyzed in this paper are collected from isolated convective clouds, so the convective bubbles keep ascending as the clouds evolve. MCSs may have different characteristics of vertical air motion because there is continuous low level convective source. The maximum vertical velocity is observed within 2 km below cloud top; this is consistent with Doppler velocity images measured by WCR (e.g. Fig. 2b), which show the typical strongest updraft is observed 1–1.5 km below cloud top. The strongest downdrafts are sometimes observed more than 2 km below cloud top. The 10% and 50% values do not have obvious trend as the clouds evolve, possibly because of the increasing contribution from moderate and weak drafts as the clouds become deeper and broader (Fig. 6 and 7). The air mass flux (Fig. 12d-f) has no obvious trend as the clouds evolve, again suggesting multiple factors (e.g. entrainment/detainment, microphysics) have impact on the evolution of the drafts. Since the aircraft just provides a line of data through drafts, and not vertical information unless the plane makes multiple passes through the same cell, more data, including remote sensing measurements are needed to better understand the evolution of the vertical velocity in convective clouds at different stages.

5. Discussion

In this study, we provide the statistics of vertical air motion in isolated convective clouds using in-situ measurements from three field campaigns. The statistical results suggest vertical air motions in convective clouds are very complicated and could be affected by many factors.

549 Microphysics strongly interacts with vertical velocity through different processes, for example,
550 droplet condensation/evaporation, ice nucleation/sublimation, water loading, etc. Yang et al.
551 (2016) shows the LWC and IWC are both higher in stronger updrafts in developing convective
552 clouds, while the liquid fraction has no obvious correlation with vertical velocity. In mature
553 convective clouds the LWC is also higher in stronger updrafts, but the IWC is similar in
554 relatively weak and strong updrafts, the liquid fraction is correlated to the vertical velocity
555 between -3 C and -8 C, possibly because Hallet-Mossop process is more significant in weaker
556 updrafts (Heymsfield and Willis, 2014). Lawson et al. (2015) shows the existence of millimeter
557 drops in the convective clouds can result in fast ice initiation, and the significant latent heat
558 released during the ice initiation process can strengthen the updrafts. In ICE-T and COPE, we do
559 observe many millimeter drops, which may strongly interact with vertical velocity through fast
560 ice generation. However, in some cases, the existence of millimeter drops can result in strong
561 warm rain process (Yang et al. 2016; Leon et al. 2016), which may weaken the updrafts and
562 make the clouds dissipate quickly.

563 Entrainment/detrainment also has strong interaction with the vertical velocity. In the analysis
564 above, we see the downdrafts in HiCu and COPE are obviously stronger than those in ICE-T.
565 This maybe partly because the ambient relative humidity is low in HiCu and COPE compared to
566 ICE-T, resulting in a strong evaporation-cooling effect when ambient air mixes with cloud
567 parcels through lateral entrainment/detrainment (Heymsfield et al., 1978). Entrainment has
568 impact on updrafts as well. Recent study using in-situ measurement and model simulation
569 suggests stronger entrainment may result in weaker updrafts (Lu et al., 2016). In ICE-T, we also
570 find the weaker updrafts are associated with stronger entrainment/detrainment using in-situ
571 measurements of relative humidity, equivalent potential temperature, droplet concentration and

LWC (not shown). In COPE and HiCu, we do not have the appropriate instruments to do similar analyses. Previous studies (e.g. Heymsfield et al., 1978; Wang et al., 2013) suggest updraft cores unaffected by entrainment may exist in some convective clouds.

Again it is important to be aware of limitations of using aircraft in-situ measurements for this kind of study. More observations (in situ and remote sensing) as well as model simulations are needed to better characterize the vertical air motion in convective clouds and its interactions with microphysics and entrainment/detrainment mixing.

6. Conclusions

The vertical velocity and air mass flux in isolated convective clouds are statistically analyzed in this study using aircraft data collected from three field campaigns, HiCu, COPE and ICE-T, conducted over mid-latitude High Plains, mid-latitude coastal area and tropical ocean. Three thresholds of air mass flux are selected to delineate weak, moderate and strong draft: 10 kg m^{-1} s^{-1}, 100 kg m^{-1} s^{-1} and 500 kg m^{-1} s^{-1} in magnitude. These definitions only apply for the isolated convective cloud in this study and are not necessarily appropriate for other convections (e.g. MCSs). The main findings are as follows.

1) Small-scale updrafts and downdrafts in convective clouds are often observed in the three field campaigns. More than 85%, 90% and 74% of the updrafts are narrower than 500 m in HiCu, COPE and ICE-T, respectively, and more than 90 % of the downdrafts are narrower than 500 m in the three field campaigns combined. These small scale drafts make significant contributions to the total air mass flux. Updrafts narrower than 500 m contribute 20%–35% of the total upward

flux, and downdrafts narrower than 500 m contribute 50%–65% of the total downward air mass flux.

2) In terms of the air mass flux, the weak and moderate drafts make an important contribution to the total air mas flux exchange. Generally, the number of drafts increases with cloud diameter. For many narrow clouds, the weak and moderate drafts dominate and contribute most of the total air mass flux. For broader clouds, the stronger updrafts contribute most of the total air mass flux, but the contribution from weak and moderate drafts increases as the cloud evolves.

3) PDFs and profiles of the vertical velocity are provided for the drafts. In all the height ranges, the PDFs are roughly exponentially distributed and broaden with height. The downdrafts are stronger in HiCu and COPE compared to ICE-T. Relatively strong updrafts (> 20 m s^{-1}) were sampled during ICE-T and COPE. The updrafts in HiCu are weaker than previous studies of deeper continental convections, possibly because the clouds sampled in HiCu were isolated convective clouds over high plains, which could be different than deeper convective clouds from low elevations.

4) PDFs and profiles of the air mass flux are provided for the drafts. The PDFs are similarly exponentially distributed at different heights, and have no obvious trend with height. In the updrafts, the maximum air mass flux has an order of 10^4 kg m^{-1} s^{-1}. The air mass flux in the downdrafts are typically a few times smaller in magnitude than those in the updrafts.

5) The composite structures of the vertical velocity in the updrafts and downdrafts have similar normalized shapes for the three field campaigns: the vertical velocity is the strongest near the center, and weakens towards the edges. Statistically, the vertical velocity and diameter were

increasing with height, but the air mass flux does not has obvious trend with height, suggesting entrainment/detrainment, water loading and other complicated processes have impacts on the evolution of the drafts.

6) The change of vertical air motion characteristics as the cloud evolves are briefly discussed. Generally, the strongest portion of a draft ascends with height as the cloud evolves. The maximum vertical velocity is observed within 2 km below cloud top; the downdrafts are sometimes stronger at levels more than 2 km below cloud top.

The vertical air motion in convective clouds is very complicated, and is affected by many factors, such as convection mechanisms, entrainment/detrainment and microphysics. This study only deals with isolated convective clouds and there are several limitations associated with using aircraft in-situ measurements. More data, including in-situ and remote sensing measurements, are needed to better understand the vertical air motion in convective clouds.

Acknowledgments

This work is supported by National Science Foundation Award: AGS-1230203 and AGS-1034858, the National Basic Research Program of China under grant no. 2013CB955802 and DOE Grant DE-SC0006974 as part of the ASR program. The authors acknowledge the crew of NCAR C-130 and University of Wyoming King Air for collecting the data and for providing high-quality products. Many thanks are also extended to the two reviewers for their constructive comments.

References

Anderson, N. F., Grainger, C. A., and Stith, J. L.: Characteristics of Strong Updrafts in Precipitation Systems over the Central Tropical Pacific Ocean and in the Amazon. J. Appl. Meteor., 44, 731–738, 2005.

Arakawa, A.: The cumulus parameterization problem: Past, present, and future. J. Clim., 17, 2493–2525, 2004.

Bechtold, P., Bazile, E., Guichard, F., Mascart, P. and Richard, E.: A mass-flux convection scheme for regional and global models. Quarterly Journal of the Royal Meteorological Society, 127(573), 869-886, 2001.

Byers, H. R. and Braham, R. R.: The Thunderstorm-Report of the Thunderstorm Project. U.S. Weather Bureau, Washington, D.C., Jun 1949. 287 pp. [NTIS PB234515], 1949.

Del Genio, A. D., Wolf, A. B., and Yao, M.-S.: Evaluation of regional cloud feedbacks using single-column models, J. Geophys. Res., 110, D15S13, doi:10.1029/2004JD005011, 2005.

Collis, S., Protat, A., May, P. T., and Williams, C.: Statistics of Storm Updraft Velocities from TWP-ICE Including Verification with Profiling Measurements. J. Appl. Meteor. Climatol., 52, 1909–1922, 2013.

Donner, L. J., Seman, C. J., Hemler, R. S., and Fan, S.: A Cumulus Parameterization Including Mass Fluxes, Convective Vertical Velocities, and Mesoscale Effects: Thermodynamic and Hydrological Aspects in a General Circulation Model. J. Climate, 14, 3444–3463, 2001.

Giangrande, S. E., Collis, S., Straka, J., Protat, A., Williams, C. and Krueger, S.: A summary of convective-core vertical velocity properties using ARM UHF wind profilers in Oklahoma. J. App. Meteor. Climatol., 52, 2278-2295, 2013.

Heymsfield, A. J., Johnson, P. N., and Dye, J. E.: Observations of Moist Adiabatic Ascent in Northeast Colorado Cumulus Congestus Clouds. J. Atmos. Sci., 35, 1689–1703, 1978.

Heymsfield, A. J., and Willis, P.: Cloud conditions favoring secondary ice particle production in tropical maritime convection. J. Atmos. Sci., 71, 4500–4526, 2014.

Heymsfield, G. M., Tian, L., Heymsfield, A. J., Li, L., and Guimond, S.: Characteristics of Deep Tropical and Subtropical Convection from Nadir-Viewing High-Altitude Airborne Doppler Radar. J. Atmos. Sci., 67, 285–308, 2010.

Hildebrand, P. H., Lee, W., Walther, C. A., Frush, C., Randall, M., Loew, E., Neitzel, R., and Parsons, R.: The ELDORA/ASTRAIA Airborne Doppler Weather Radar: High-Resolution Observations from TOGA COARE. *Bull. Amer. Meteor. Soc.*, 77, 213–232, 1996

Hogan, R. J., Grant, A. L., Illingworth, A. J., Pearson, G. N., and O'Connor, E. J.: Vertical velocity variance and skewness in clear and cloud-topped boundary layers as revealed by Doppler lidar, Q. J. Roy. Meteorol. Soc., 135, 635–643, 2009.

Houze Jr., R. A., and Betts, A. K.: Convection in GATE, Rev. Geophys., 19(4), 541–576, 1981.

Igau, R. C., LeMone, M. A., and Wei, D.: Updraft and Downdraft Cores in TOGA COARE: Why So Many Buoyant Downdraft Cores?. J. Atmos. Sci., 56, 2232–2245, 1999.

Ivanova, I. T. and Leighton, H. G.: Aerosol–Cloud Interactions in a Mesoscale Model. Part I: Sensitivity to Activation and Collision–Coalescence. J. Atmos. Sci., 65, 289–308, 2008.

Jorgensen, D. P., Zipser, E. J., and LeMone, M. A.: Vertical Motions in Intense Hurricanes. J. Atmos. Sci., 42, 839–856, 1985.

Jorgensen, D. P. and LeMone, M. A.: Vertically Velocity Characteristics of Oceanic Convection. J. Atmos. Sci., 46, 621–640, 1989.

Jorgensen, D. P., and Smull, B. F.: Mesovortex circulations seen by airborne Doppler radar within a bow-echo mesoscale convective system. Bull. Amer. Meteor. Soc., **74,** 2146–2157, 1993.

Jorgensen, D. P., Shepherd, T. R., and Goldstein, A. S.: A dual-pulse repetition frequency scheme for mitigating velocity ambiguities of the NOAA P-3 airborne Doppler radar. J. Atmos. Oceanic Technol., **17,** 585–594, 2000.

Khairoutdinov, M. F., Krueger, S. K., Moeng, C.-H., Bogenschutz, P. A., and Randall, D. A.: Large-Eddy Simulation of Maritime Deep Tropical Convection, J. Adv. Model. Earth Syst., 1, 15, doi:10.3894/JAMES.2009.1.15, 2009.

Khelif, D., Burns, S. P., and Friehe, C. A.: Improved Wind Measurements on Research Aircraft. J. Atmos. Oceanic Technol., 16, 860–875, 1999.

Kollias, P and Albrecht, B.: Vertical Velocity Statistics in Fair-Weather Cumuli at the ARM TWP Nauru Climate Research Facility. J. Climate, 23, 6590–6604, 2010.

693 Lawson, P. R., Woods, S., and Morrison, H.: The microphysics of ice and precipitation
694 development in tropical cumulus clouds. J. Atmos. Sci., 72, 2429-2445, 2015.

695 LeMone, M. A., and Zipser, E. J.: Cumulonimbus vertical velocity events in GATE. Part I:
696 Diameter, intensity and mass flux. J. Atmos. Sci., 37, 2444–2457, 1980.

697 Leon, D., and co-authors: The COnvective Precipitation Experiment (COPE): Investigating the
698 origins of heavy precipitation in the southwestern UK. Bull. Amer. Meteor. Soc.
699 doi:10.1175/BAMS-D-14-00157.1, in press, 2016.

700 Lu, C., Liu, Y., Zhang, G. J., Wu, X., Endo, S., Cao, L., Li, Y. and Guo, X.: Improving
701 parameterization of entrainment rate for shallow convection with aircraft measurements and
702 large eddy simulation. J. Atmos. Sci., 2015.

703 Lucas, C., Zipser, E. J., and Lemone, M. A.: Vertical Velocity in Oceanic Convection off
704 Tropical Australia. J. Atmos. Sci., 51, 3183–3193, 1994.

705 May, P. T. and Rajopadhyaya, D. K.: Vertical Velocity Characteristics of Deep Convection over
706 Darwin, Australia. Mon. Wea. Rev., 127, 1056–1071, 1999.

707 Nicol, J. C., Hogan, R. J., Stein, T. H. M., Hanley, K. E., Clark, P. A., Halliwell, C. E., Lean, H.
708 W., and Plant, R. S.: Convective updraught evaluation in high-resolution NWP simulations using
709 single-Doppler radar measurements. Q. J. R. Meteorol. Soc., 141, 3177–3189, 2015.

710 Schmeter, S. M.: Structure of fields of meteorological elements in a cumulonimbus zone, Hydro.
711 Meteor. Serv., Trans. Cent. Aerol. Obs. [Trans. From Russian by Israel Prog. For Sci. Trans.,
712 Jerusalem, 1970, 117 pp.], 1969.

713 Schumacher, C., Stevenson, S. N., and Williams, C. R.: Vertical motions of the tropical
714 convective cloud spectrum over Darwin, Australia. Q.J.R. Meteorol. Soc.. doi: 10.1002/qj.2520,
715 2015.

716 Tiedtke, M.: A comprehensive mass flux scheme for cumulus parameterization in large-scale
717 models. Monthly Weather Review, 117(8), 1779-1800, 1989.

718 Tonttila, J., O'Connor, E. J., Niemelä, S., Räisänen, P., and Järvinen, H.: Cloud base vertical
719 velocity statistics: a comparison between an atmospheric mesoscale model and remote sensing
720 observations. Atmos. Chem. Phys., 11, 9207-9218, 2011.

721 Wang, X., and Zhang M.: Vertical velocity in shallow convection for different plume types, J.
722 Adv. Model. Earth Syst., 6, 478–489, 2014.

723 Wang, Y. and Geerts, B.: Composite Vertical Structure of Vertical Velocity in Nonprecipitating
724 Cumulus Clouds. Mon. Wea. Rev., 141, 1673–1692, 2013.

725 Wang, Z. and co-authors: Single aircraft integration of remote sensing and in situ sampling for
726 the study of cloud microphysics and dynamics. Bull. Amer. Meteor. Soc., 93, 653–668, 2012.

727 Weisman, M. L. and Klemp, J. B.: The dependence of numerically simulated convective storms
728 on vertical wind shear and buoyancy. Monthly Weather Review, 110, 504-520, 1982.

729 Wendisch, M., and Brenguier, J.: Airborne Measurements for Environmental Research: Methods
730 and Instruments. Wiley, 520 pages, 2013.

Wu, J., Del Genio, A. D., Yao, M.-S., and Wolf, A. B.: WRF and GISS SCM simulations of convective updraft properties during TWP-ICE, J. Geophys. Res., 114, D04206, doi:10.1029/2008JD010851, 2009.

Yang, J., Wang, Z., Heymsfield, A. J., and Luo, T.: Liquid/Ice Mass Partition in Tropical Maritime Convective Clouds. J. Atmos. Sci., in review, 2016.

Zipser, E. J., Cecil, D. J., Liu, C., Nesbitt, S. W., and Yorty, D. P.: Where are the most intense thunderstorms on Earth?. Bull. Amer. Meteor. Soc., 87, 1057–1071, 2006.

Table 1. Number of penetrations, time in clouds and flight length in clouds sampled at 0–2 km, 2–4 km, 4–6 km, 6–8 km and 8–10 km MSL in HiCu, COPE and ICE-T.

Height (km MSL)	HiCu			COPE			ICE-T		
	Number of penetrations	Time in clouds (min)	Length in clouds (km)	Number of penetrations	Time in clouds (min)	Length in clouds (km)	Number of penetrations	Time in clouds (min)	Length in clouds (km)
8–10	43	12	79						
6–8	565	122	789				132	52	423
4–6	596	104	653	207	39	244	299	116	895
2–4	373	50	274	378	86	486	34	10	73
0–2				219	40	211	197	27	167

Table 2. Number of updrafts and downdrafts sampled at 0-2 km, 2-4 km, 4-6 km, 6-8 km and 8-10 km in HiCu, COPE and ICE-T. Three numbers are given for the updraft and downdraft at each level, respectively, according to the three different definitions: weak, moderate and strong.

Height (km)		HiCu		COPE		ICE-T	
		Updraft	Downdraft	Updraft	Downdraft	Updraft	Downdraft
8-10	weak	66	100				
	moderate	52	44				
	strong	44	17				
6-8	weak	818	763			382	372
	moderate	559	540			175	136
	strong	287	130			102	23
4-6	weak	748	668	290	184	858	671
	moderate	522	389	232	193	425	329
	strong	343	48	135	51	266	73
2-4	weak	311	235	568	424	49	47
	moderate	271	84	467	434	51	51
	strong	149	7	188	101	32	10
0-2	weak			368	192	319	205
	moderate			266	90	234	104
	strong			96	9	60	7

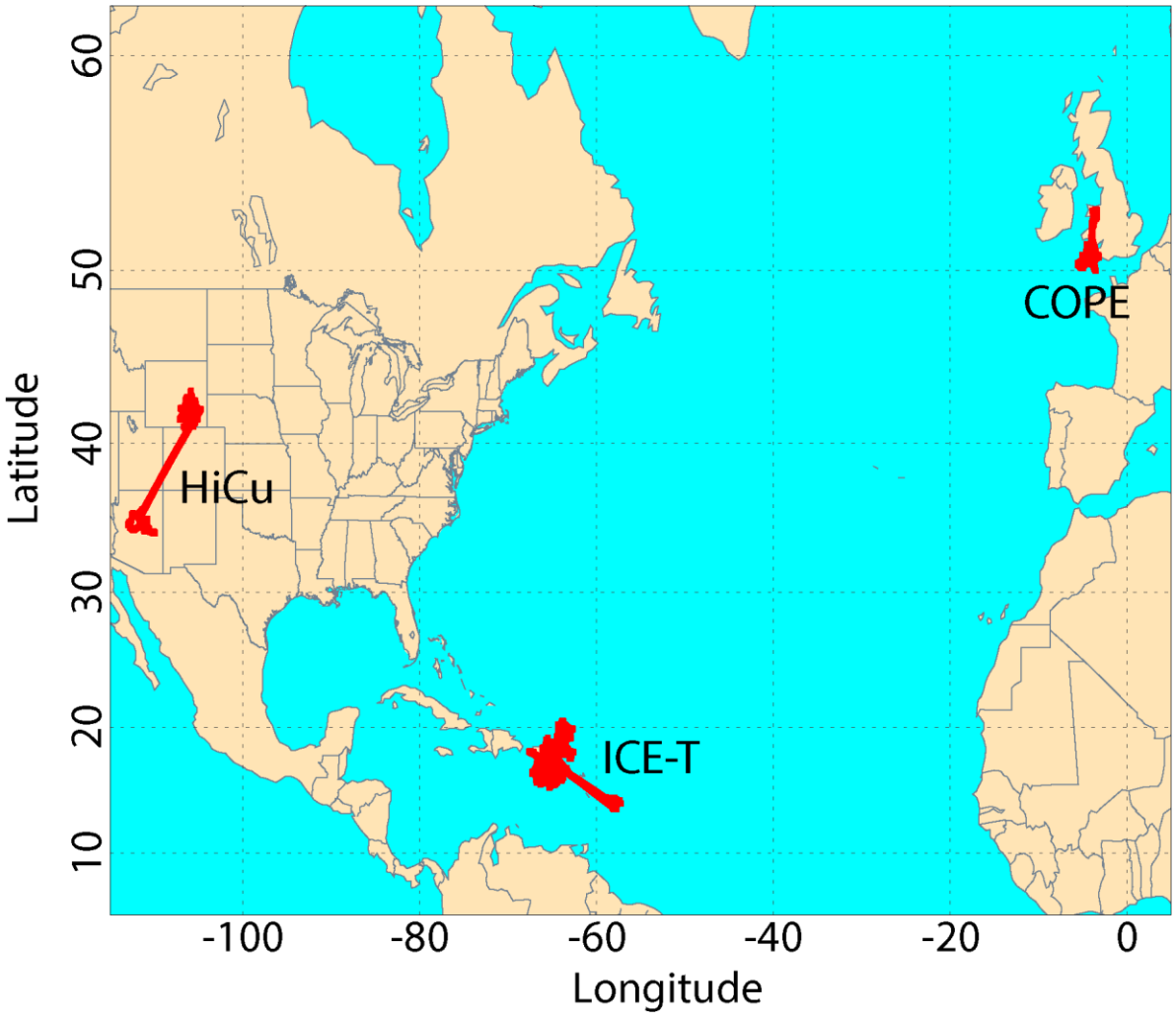

Figure 1. Flight tracks for the three field campaigns: HiCu, COPE and ICE-T.

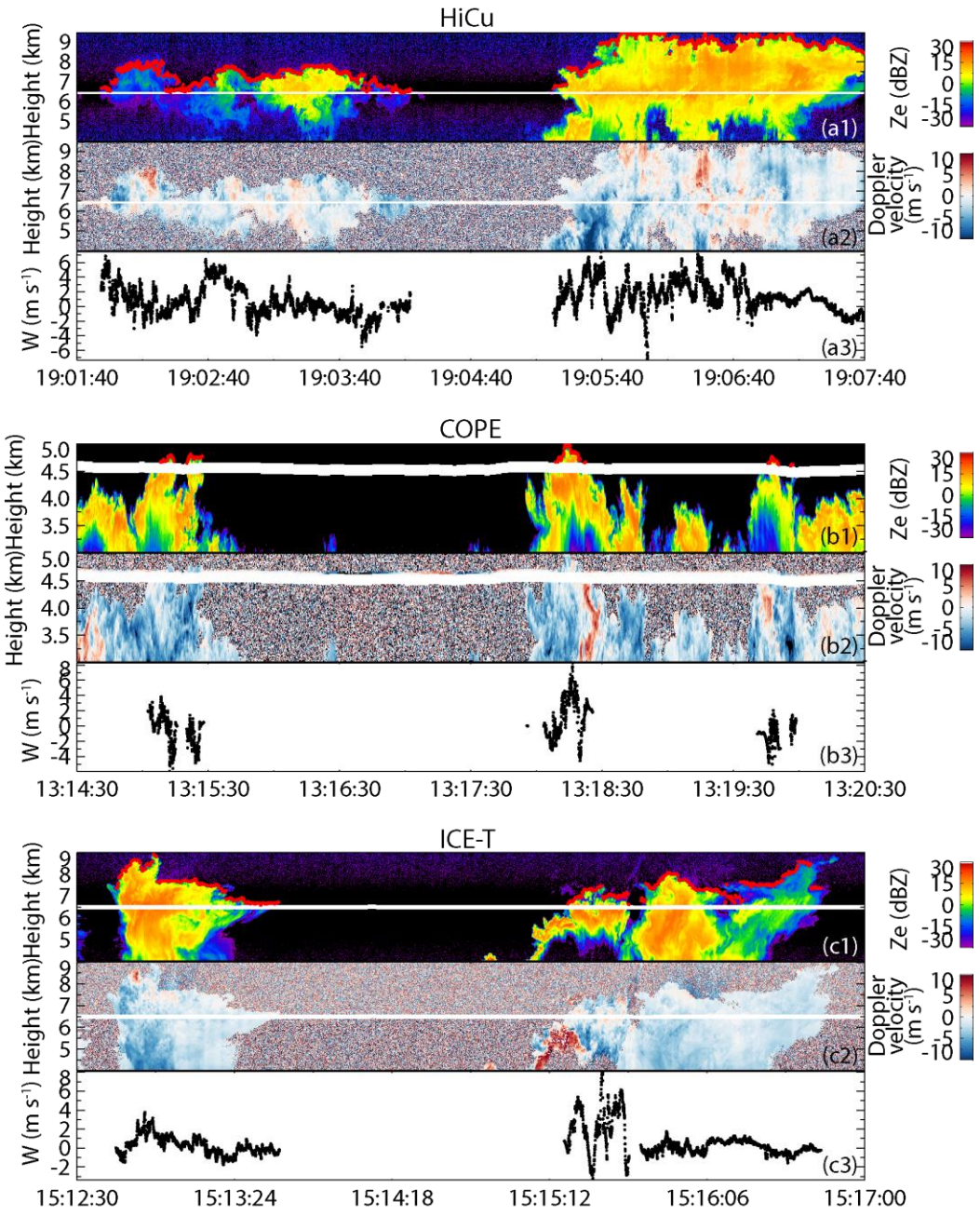

Figure 2. Examples of radar reflectivity, Doppler velocity and 25-Hz in-situ vertical velocity measurements for the convective clouds sampled in HiCu, COPE and ICE-T. The red dots in (a1), (b1) and (c1) are the cloud tops estimated by WCR.

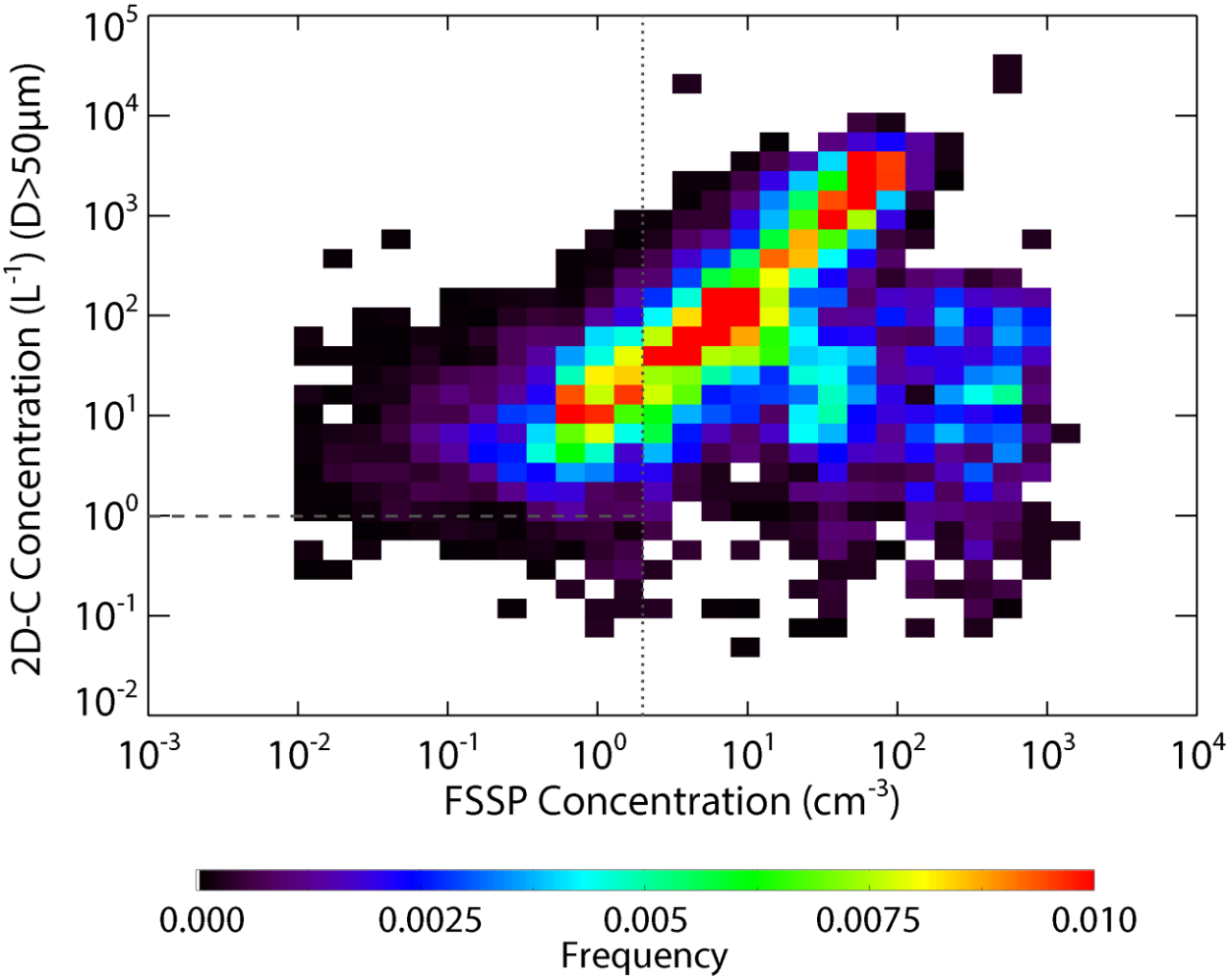

Figure 3. Occurrence distributions as a function of the particle concentrations measured by FSSP versus the concentrations of the particles ≥ 50 μm in diameter measured by 2D-C in the clouds identified by WCR reflectivity. The dashed and dotted lines indicate the FSSP concentration equal 2 cm^{-3} and the 2D-C concentration equal 1 L^{-1}, respectively.

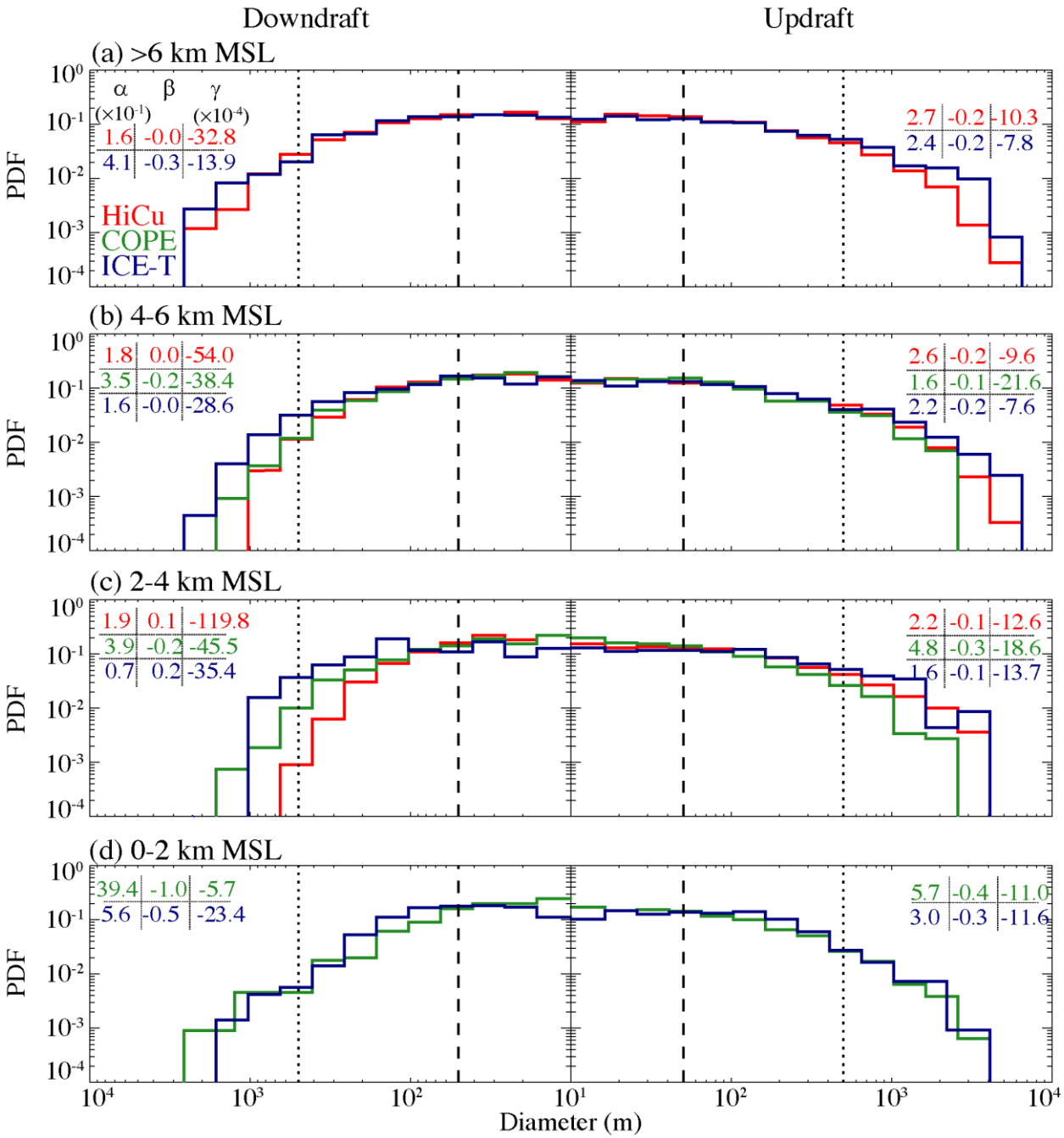

Figure 4. PDFs of the diameters for the updrafts and downdrafts sampled at 0–2 km, 2–4 km, 4–6 km and higher than 6 km. The numbers shown in each panel are the coefficients of the fitted exponential function (Eq. 1).

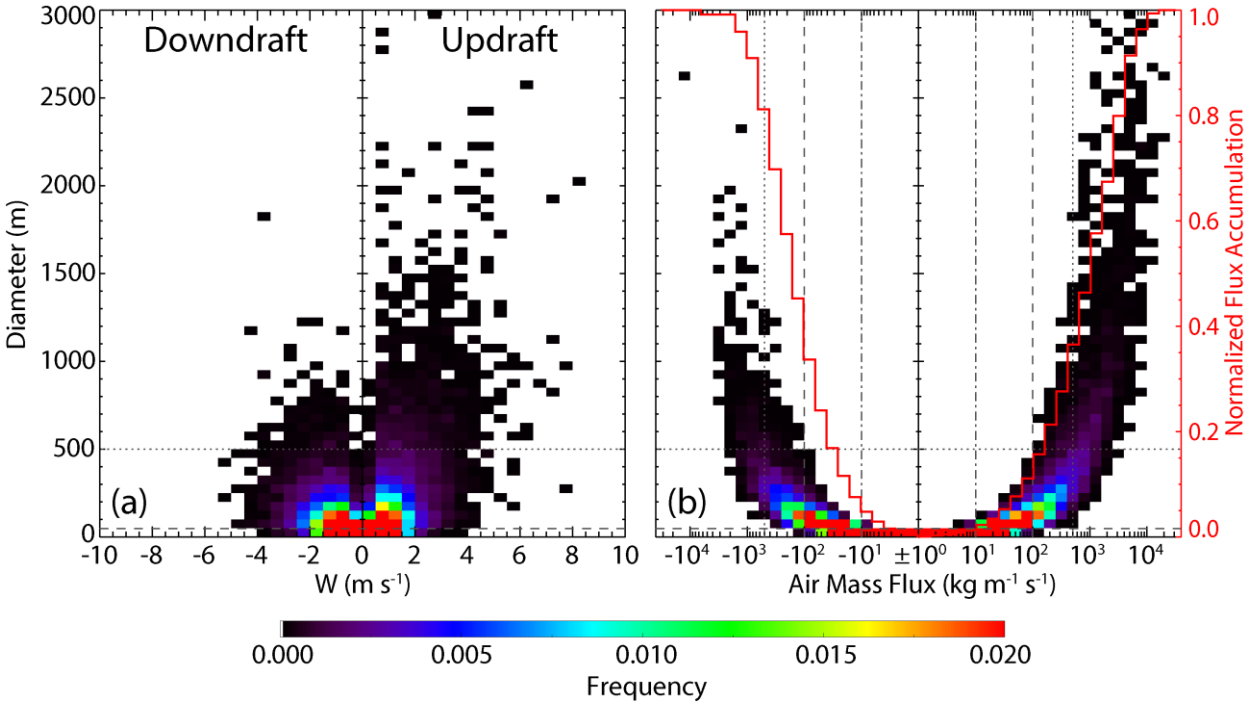

Figure 5. Occurrence distributions as (a) a function of diameter and mean vertical velocity, and (b) a function of diameter and air mass flux for all updrafts and downdrafts. The normalized accumulation flux is also shown by the red curves. The horizontal dotted and dashed lines in (a) and (b) indicate the draft diameter equal 500 m and 50 m, which are used as the diameter thresholds to identify a "draft" in previous studies and in this study, respectively. The vertical dash-dotted, dashed and dotted lines in (b) indicate air mass flux equal 10 kg m^{-1} s^{-1}, 100 kg m^{-1} s^{-1} and 500 kg m^{-1} s^{-1} in magnitude, respectively, which are the thresholds used to delineate the three different groups of draft.

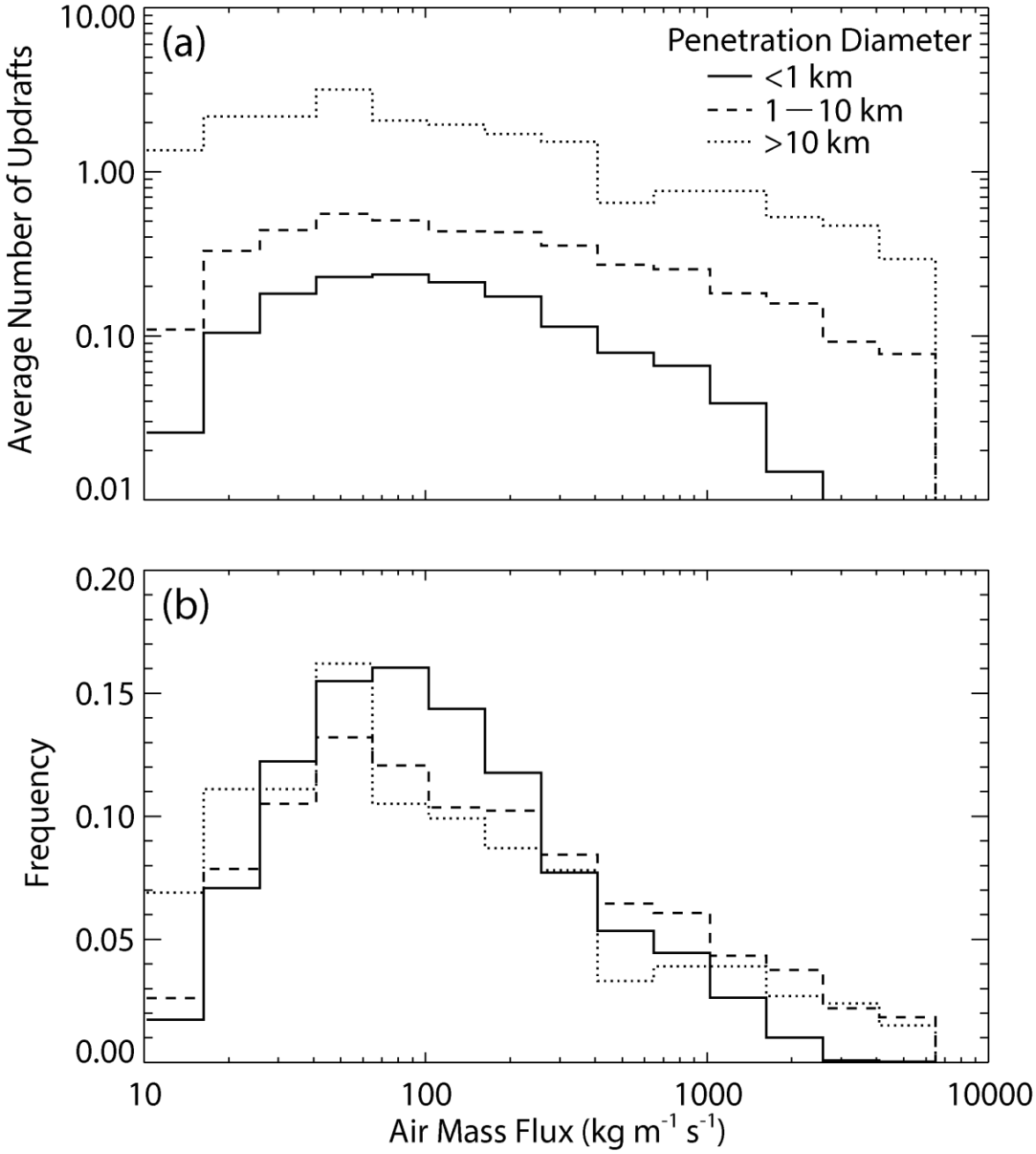

Figure 6. (a) Average number and (b) occurrence frequency of updrafts as a function of air mass flux observed in penetrations with length < 1 km (solid), 1-10 km (dashed) and >10 km (dotted). The result is a composite of HiCu, COPE and ICE-T.

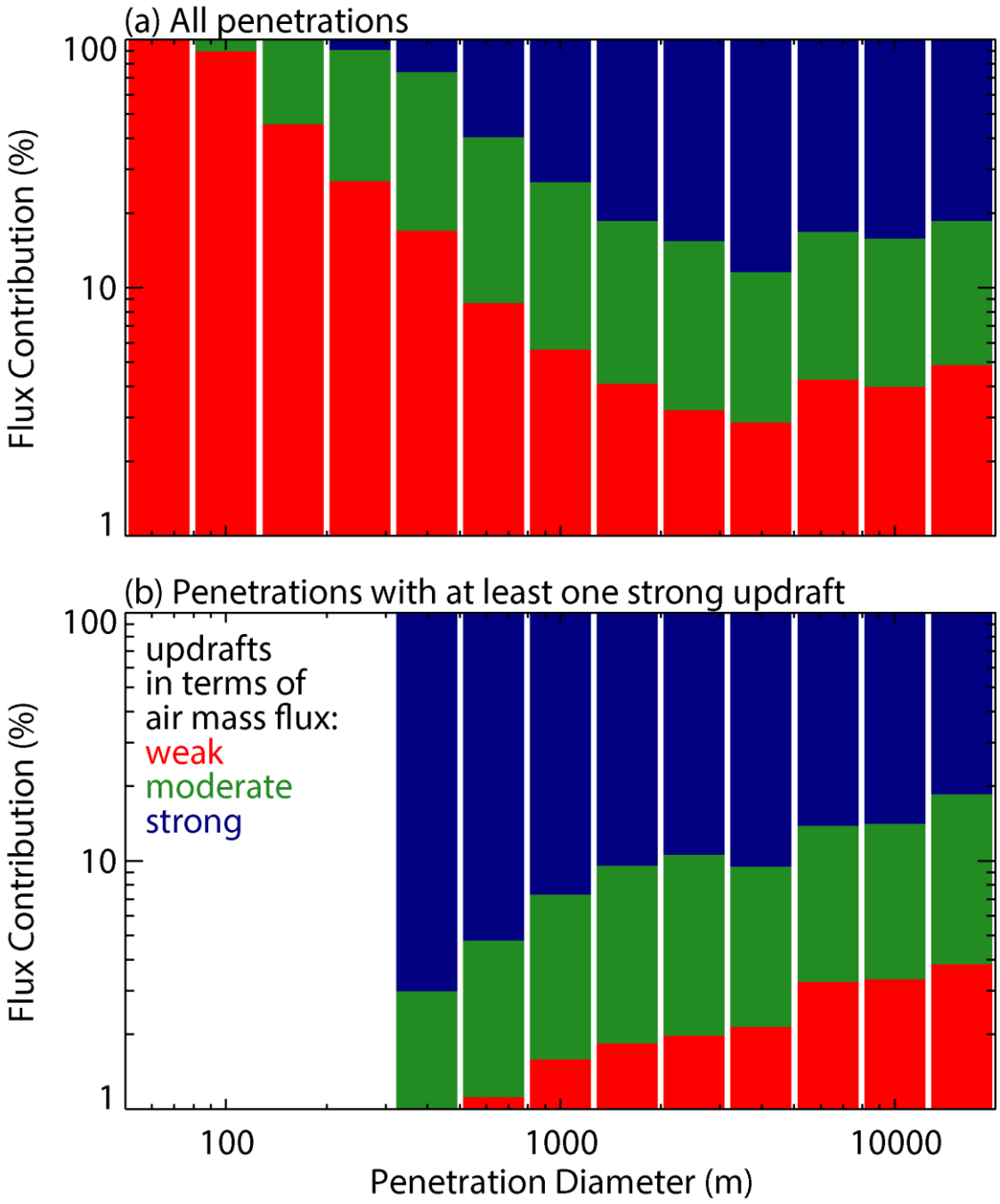

Figure 7. Average percentile contribution to total upward air mass flux by the weak (red), moderate (green) and strong (blue) updrafts delineated in this study. The result is a composite of HiCu, COPE and ICE-T.

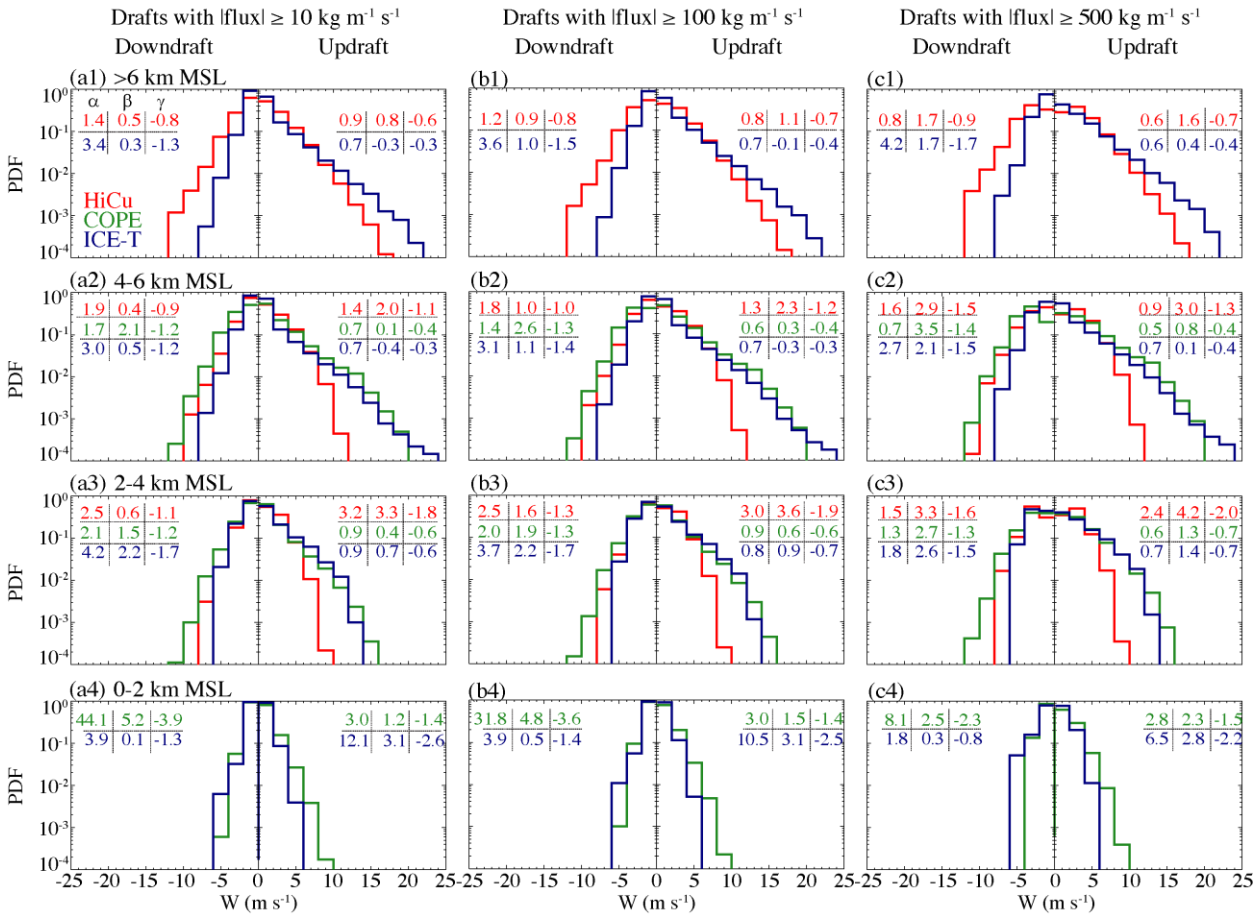

Figure 8. PDFs of the 25-Hz vertical velocity for the updrafts and downdrafts with air mass flux ≥ (a) 10 kg m^{-1} s^{-1}, (b) 100 kg m^{-1} s^{-1} and (c) 500 kg m^{-1} s^{-1} in magnitude, sampled at 0–2 km, 2–4 km, 4–6 km and higher than 6 km. The numbers shown in each panel are the coefficients of the fitted exponential function (Eq. 1).

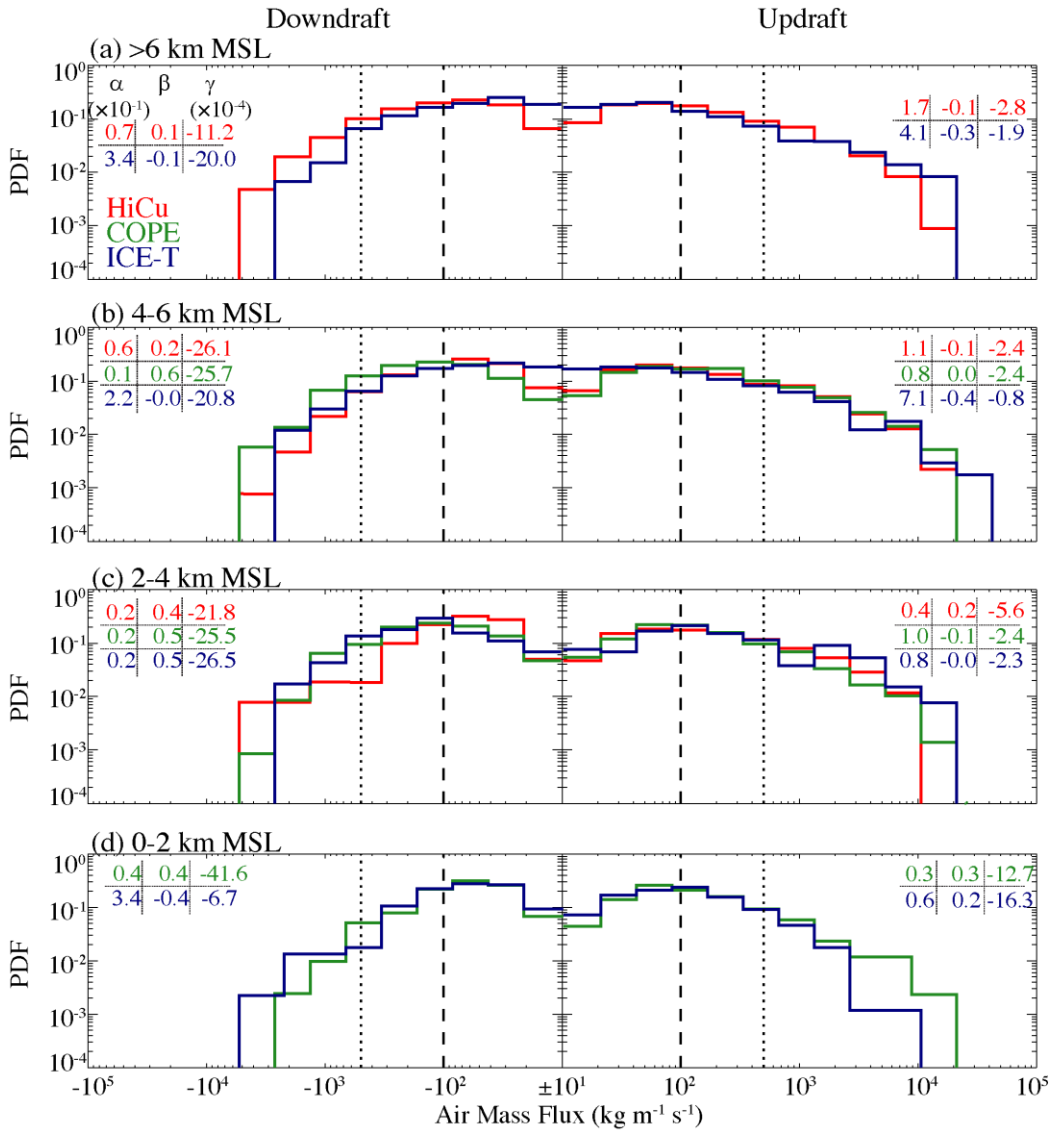

Figure 9. PDFs of the air mass flux for the updrafts and downdrafts sampled at 0–2 km, 2–4 km, 4–6 km and higher than 6 km. The three thresholds of the air mass flux (±10 kg m^{-1} s^{-1}, ±100 kg m^{-1} s^{-1} and ±500 kg m^{-1} s^{-1}) are shown by the solid (overlaps with the central y-axis in each panel), dashed and dotted lines. The numbers shown in each panel are the coefficients of the fitted exponential function (Eq. 1).

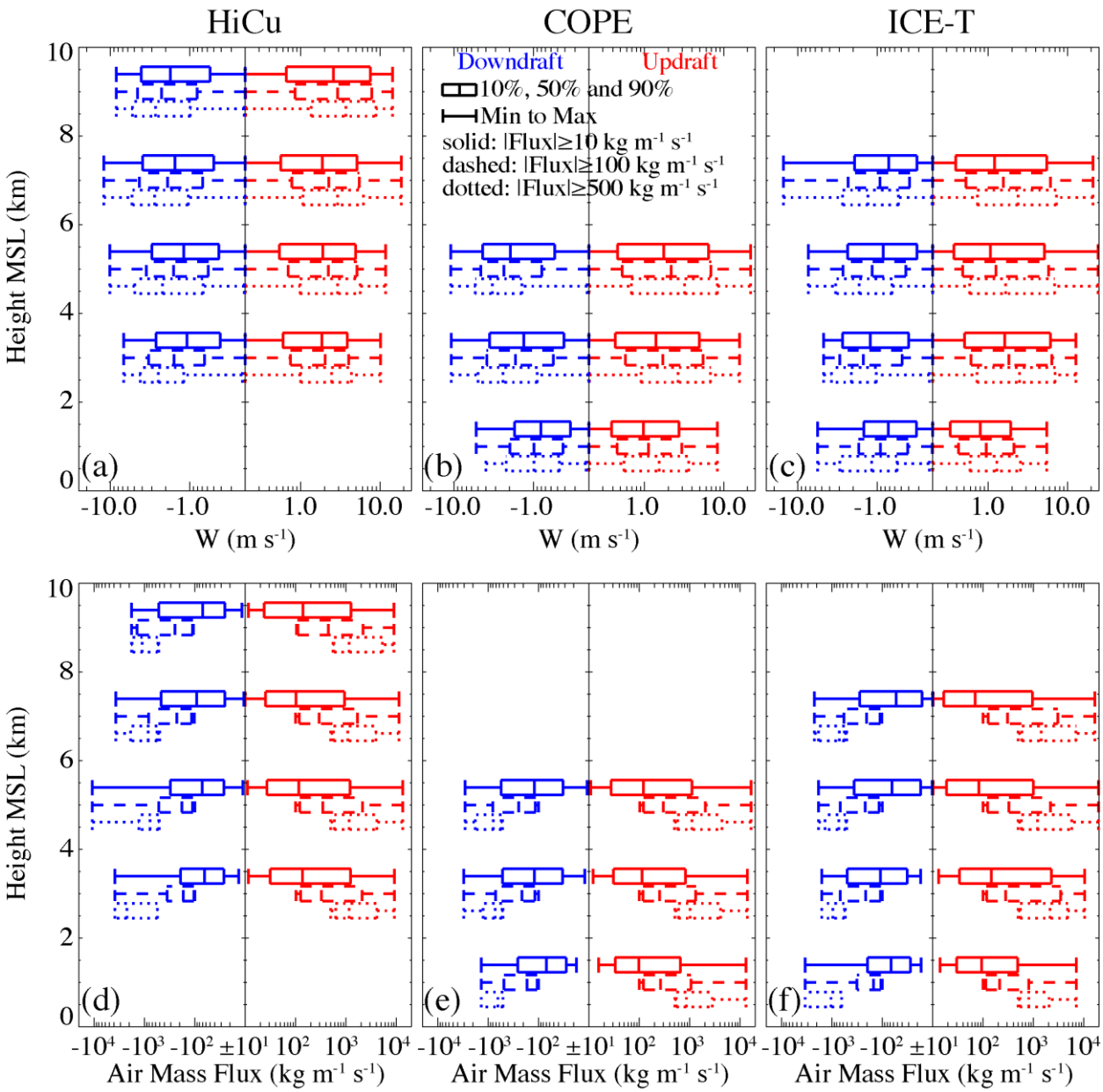

Figure 10. Profiles of (a-c) the vertical velocity and (d-f) air mass flux for all the updrafts and downdrafts sampled at 0–2 km, 2–4 km, 4–6 km, 6–8 km and 8–10 km. The dotted, dashed and solid boxes represent for the drafts with air mass flux ≥ 10 kg m^{-1} s^{-1}, 100 kg m^{-1} s^{-1} and 500 kg m^{-1} s^{-1} in magnitude, respectively.

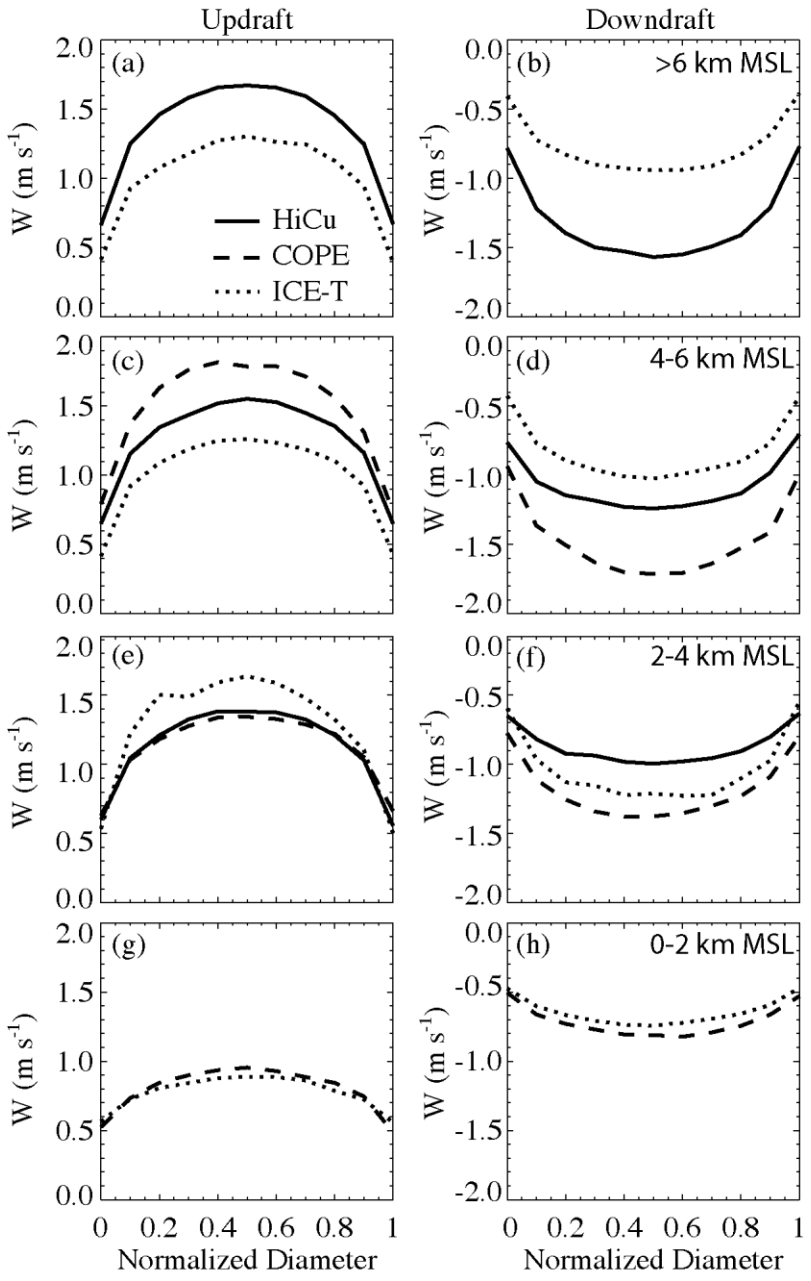

Figure 11. Composite structure of the vertical velocity as a function of the normalized diameter for the updrafts and downdrafts with air mass flux ≥ 10 kg m^{-1} s^{-1} in magnitude. The 0 and 1 coordinates on the x-axis indicate the upwind and downwind sides of the draft.

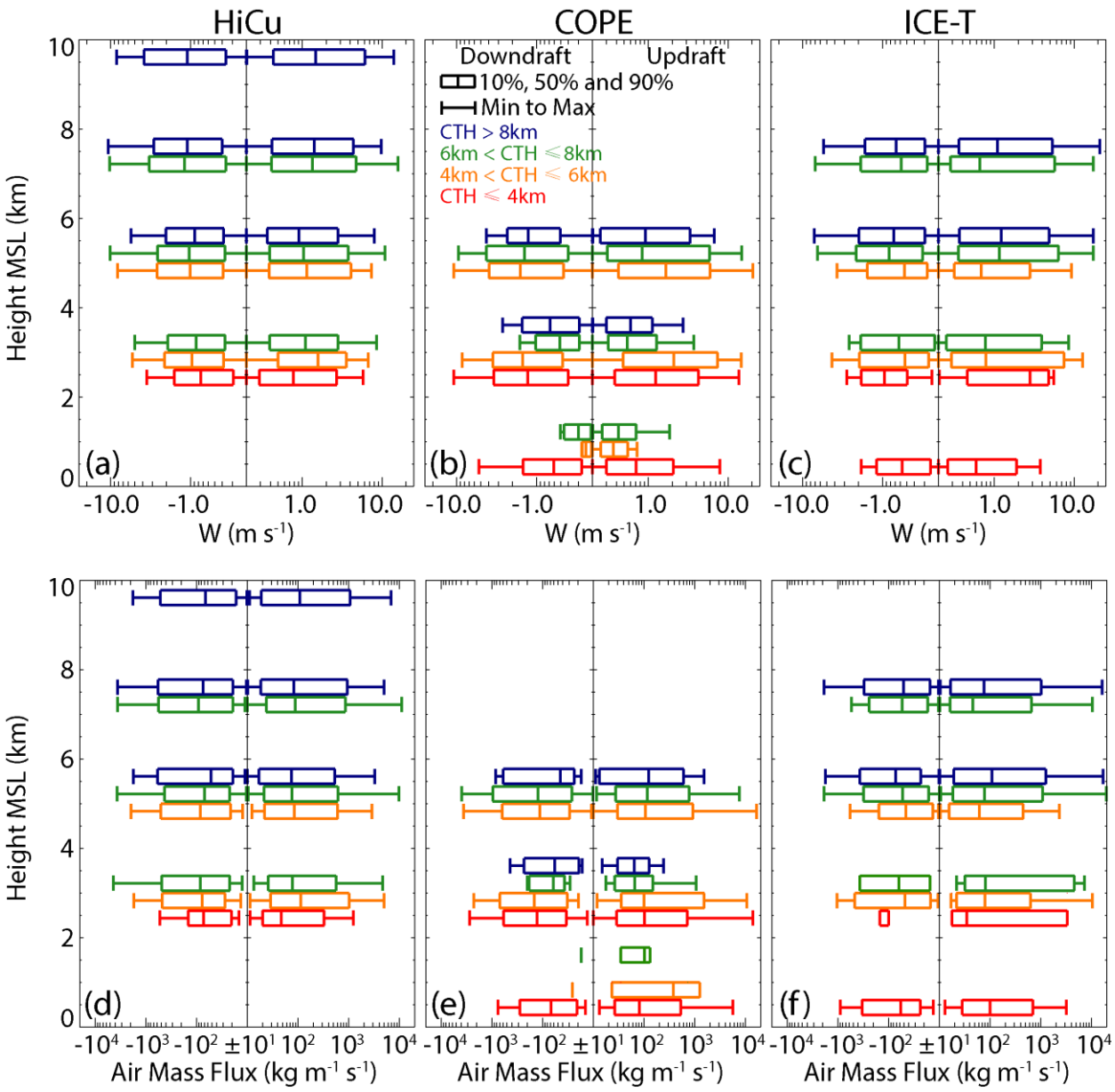

Figure 12. Profiles of (a-c) the vertical velocity and (d-f) the air mass flux for the updraft and downdraft with air mass flux ≥ 10 kg m^{-1} s^{-1} in magnitude. The red, orange, green and blue boxes represent clouds with cloud top heights of 0-4 km, 4-6 km, 6-8 km and higher than 8 km.